# Ionic mechanisms of autorhythmic firing in rat cerebellar Golgi cells

Lia Forti, Elisabetta Cesana, Jonathan Mapelli and Egidio D'Angelo

*Dipartimento di Scienze Fisiologiche e Farmacologiche and Istituto Naz. Fisica della Materia, Università di Pavia, Via Forlanini 6, 27100 Pavia, Italy*

**Although Golgi cells (GoCs), the main type of inhibitory interneuron in the cerebellar granular layer (GL), are thought to play a central role in cerebellar network function, their excitable properties have remained unexplored. GoCs fire rhythmically *in vivo* and in slices, but it was unclear whether this activity originated from pacemaker ionic mechanisms. We explored this issue in acute cerebellar slices from 3-week-old rats by combining loose cell-attached (LCA) and whole-cell (WC) recordings. GoCs displayed spontaneous firing at 1–10 Hz (room temperature) and 2–20 Hz (35–37°C), which persisted in the presence of blockers of fast synaptic receptors and mGluR and $GABA_B$ receptors, thus behaving, in our conditions, as pacemaker neurons. ZD 7288 (20 $\mu$M), a potent hyperpolarization-activated current ($I_h$) blocker, slowed down pacemaker frequency. The role of subthreshold $Na^+$ currents ($I_{Na,sub}$) could not be tested directly, but we observed a robust TTX-sensitive, non-inactivating $Na^+$ current in the subthreshold voltage range. When studying repolarizing currents, we found that retigabine (5 $\mu$M), an activator of KCNQ $K^+$ channels generating neuronal M-type $K^+$ ($I_M$) currents, reduced GoC excitability in the threshold region. The KCNQ channel antagonist XE991 (5 $\mu$M) did not modify firing, suggesting that GoC $I_M$ has low XE991 sensitivity. Spike repolarization was followed by an after-hyperpolarization (AHP) supported by apamin-sensitive $Ca^{2+}$-dependent $K^+$ currents ($I_{apa}$). Block of $I_{apa}$ decreased pacemaker precision without altering average frequency. We propose that feed-forward depolarization is sustained by $I_h$ and $I_{Na,sub}$, and that delayed repolarizing feedback involves an $I_M$-like current whose properties remain to be characterized. The multiple ionic mechanisms shown here to contribute to GoC pacemaking should provide the substrate for fine regulation of firing frequency and precision, thus influencing the cyclic inhibition exerted by GoCs onto the cerebellar GL.**

(Resubmitted 3 April 2006; accepted after revision 5 May 2006; first published online 11 May 2006)
**Corresponding author** L. Forti: Dipartimento di Scienze Fisiologiche e Farmacologiche, Università di Pavia, Via Forlanini 6, 27100 Pavia, Italy. Email: lforti@unipv.it

Inhibitory interneurons are key elements for network computation and learning (Singer, 1993). In the cerebellum, the main inhibitory neurons of the granular layer (GL) are Golgi cells (GoCs; Golgi, 1883). GoCs are activated by mossy and parallel fibres, and are inhibited by molecular layer interneurons (Eccles *et al.* 1967) and by Lugaro cells (Dieudonné & Dumoulin, 2000). In turn, GoCs contact granule cells at glomeruli with inhibitory synapses (Eccles *et al.* 1967), thereby regulating information flow along the mossy fibre pathway. Investigations *in vivo* revealed that GoCs show spontaneous rhythmic discharge both in awake (cat: 2 to ~50 Hz, Edgley & Lidierth, 1987; monkey: 10–80 Hz, Miles *et al.* 1980) and anaesthetized animals (rat: 2 to ~30 Hz, Schulman & Bloom, 1981; Vos *et al.* 1999). An interesting observation is that the granular layer of awake animals during states of quiet attentiveness shows a population oscillatory activity at 7–8 Hz (rat; Hartmann & Bower, 1998) or 15–18 Hz (monkey; Pellerin & Lamarre, 1997). This raises the question as to whether GoC rhythmicity is driven by network oscillations or is due to intrinsic pacemaking. Answering this question is critical in view of the role played by neuronal excitability in determining network behaviours (Llinás, 1988).

The observation of GoC spontaneous discharge in cerebellar slices (~3 Hz, rat, Dieudonné, 1998; 5–20 Hz, turtle, Midtgaard, 1992) suggests that GoCs could be autorhythmic. Autorhythmicity usually requires the interplay of at least two voltage-dependent mechanisms, one causing feedforward depolarization, and the other delayed feedback repolarization (Wang & Rinzel, 1999; Hutcheon & Yarom, 2000). In low-frequency (1–10 Hz) pacemaker neurons, subthreshold $Na^+$ currents ($I_{Na,sub}$) are generally found to contribute to pacemaker

 DOI: 10.1113/jphysiol.2006.110858

depolarization (Pennartz *et al.* 1997; Feigenspan *et al.* 1998; Bevan & Wilson, 1999; Bennett *et al.* 2000; Beurrier *et al.* 2000; Wilson & Callaway, 2000; Taddese & Bean, 2002; Do & Bean, 2003; Jackson *et al.* 2004 and references therein). A contribution to this depolarization is also given, in some neuronal types, by the hyperpolarization-activated current $I_h$ (Maccaferri & McBain, 1996; Bennett *et al.* 2000; Neuhoff *et al.* 2002; Funahashi *et al.* 2003; Chan *et al.* 2004) and by voltage-dependent $Ca^{2+}$ currents with low activation threshold (Wilson & Callaway, 2000; Jackson *et al.* 2004; Pignatelli *et al.* 2005). Among feedback voltage-dependent mechanisms, a number of slow $K^+$ currents may contribute to interspike repolarization on a time scale compatible with slow pacemaking. Apamin-sensitive $Ca^{2+}$-dependent $K^+$ currents ($I_{apa}$) can regulate firing frequency and precision in several pacemaker neurons (reviewed in Stocker, 2004). Given its slow activation just below action potential (AP) threshold and its lack of inactivation (Brown & Adams, 1980; Brown & Yu, 2000), the M-type $K^+$ current ($I_M$) is also expected to regulate the interspike trajectory. Although $I_M$ functional properties in native neurons have been mainly studied in non-pacemaker cells (reviewed in Brown & Yu, 2000), immunocytochemical data suggest that KCNQ2, a member of the KCNQ (Kv7) family, which is thought to generate $I_M$ (Wang *et al.* 1998; Brown & Yu, 2000; Jentsch, 2000; Robbins, 2001), is preferentially expressed in neurons having an important role in the control of local network oscillations in various CNS areas (Cooper *et al.* 2001).

Various channels potentially relevant to pacemaker activity are suggested to be expressed in cerebellar GoCs. mRNAs coding for the $I_h$ channel subtype hcn2 (mouse; Santoro *et al.* 2000) and hcn2 protein (rat; Notomi & Shigemoto, 2004) were detected in the GL with a distribution compatible with their presence in GoCs. Transcripts coding for two members of the KCNQ family (KCNQ2 and KCNQ5; Wang *et al.* 1998; Schroeder *et al.* 2000; Saganich *et al.* 2001) were found in the rat GL, and selective expression of KCNQ2 protein was shown in putative mouse GoCs (Cooper *et al.* 2001). Finally, $I_{apa}$ is mediated by channels of the SK family, in particular SK2 and SK3 subtypes (Kohler *et al.* 1996; Ishii *et al.* 1997). In rat GoCs, mRNAs encoding the SK3 subtype are particularly abundant (Stocker & Pedarzani, 2000). Overall, these data suggested that $I_h$, $I_M$ and $I_{apa}$ could be functionally expressed in GoCs and could have a role in the control of spontaneous firing.

By performing loose cell-attached (LCA) and whole-cell (WC) recordings, we demonstrate that GoCs in acute cerebellar slices behave indeed as pacemaker neurons. Pacemaking involves the action of at least two depolarizing currents active in the subthreshold region ($I_{Na,sub}$ and $I_h$) and possibly of an M-like current contributing to the repolarizing feedback. $I_{apa}$ regulates spike after-hyperpolarization (AHP) and inter-spike interval (ISI) precision. These results bear several consequences for the mechanism of inhibition in the cerebellar circuit, and suggest that GoC pacemaking can be finely regulated by several voltage-dependent channels.

## Methods

### Slice preparation

Sagittal or parasagittal cerebellar slices (220 $\mu$m thick) were cut from the vermis of 16- to 21-day-old (P16–P21) Wistar rats, decapitated after deep anaesthesia with halothane (Sigma-Aldrich, Milan, Italy; 0·5 ml in 2 l administered for 1–2 min). All experiments were conducted in accordance with international guidelines from the European Community Council Directive 86/609/EEC on the ethical use of animals. During the slicing procedure, the cerebellar vermis was immersed in a cold (2–3°C) 'cutting' solution containing (mM): potassium gluconate 130, KCl 15, ethylene glycol-bis ($\beta$-aminoethyl ether) *N*,*N*,*N*′,*N*′-tetraacetic acid (EGTA) 0.2, *N*-2-hydroxyethyl piperazine-*N*-2-ethanesulphonic acid (Hepes) 20, glucose 10, pH 7.4 with NaOH. This solution was found to improve the viability of GoCs (Dugué *et al.* 2005). Slices were incubated for at least 1 h before recordings in oxygenated bicarbonate-buffered ('standard extracellular') saline maintained at 32°C, containing (mM): NaCl 120, KCl 2, $MgSO_4$ 1.2, $NaHCO_3$ 26, $KH_2PO_4$ 1.2, $CaCl_2$ 2, glucose 11 (pH 7.4 when equilibrated with 95%$O_2$–5%$CO_2$).

### Electrophysiological apparatus

For electrophysiological recordings, slices were transferred to the recording chamber and perfused at 1.5 ml min$^{-1}$ with oxygenated standard extracellular saline either at room temperature (RT; 20–23°C) or at higher temperatures (32–37°C), as indicated. Slices were visualized in an upright epifluorescence microscope (Axioskop 2 FS, Zeiss, Oberkochen, Germany) equipped with a ×63, 0·9 NA water-immersion objective and differential interference contrast (DIC) optics, using infrared illumination (IR; excitation filter 750 nm) and an IR CCD camera (Till Photonics, Gräfelfing, Germany). Patch pipettes were fabricated from thick-walled borosilicate glass capillaries (1154150 or 1103286; Hilgenberg, Malsfeld, Germany) by means of a Sutter P-97 horizontal puller (Sutter Instruments, Novato, CA, USA). Recordings were obtained in the LCA or WC configuration, using a MultiClamp 700A (Axon Instruments, Molecular Devices, Sunnyvale, CA, USA) or, in a few cases, an Axoclamp 200B (Axon Instruments; in the IClamp Fast mode) amplifier. Images of cells filled with the fluorescent dye Alexa Fluor 488 (Molecular Probes,

Invitrogen, S.Giuliano Milanese, Italy) were obtained using a 50 W Xe lamp (Zeiss), excitation and emission filters centred at 480 and 535 nm, and a 505 nm dichroic mirror (41001, Chroma Technology, Rockingham, VT, USA), a high-resolution digital camera (CoolSNAP HQ; Roper Scientific, Trenton, NJ, USA) and MetaMorph software (Universal Imaging Corporation, Downington, PA, USA).

### Loose cell-attached recordings

For loose cell-attached (LCA) recordings (10–50 MΩ seal resistance), patch pipettes contained the standard extracellular saline or, in a few cases, a Hepes-buffered extracellular saline (results were indistinguishable and were therefore pooled; 2–4 MΩ pipette resistance). Pipettes were held at 0 mV in the voltage-clamp mode. Consecutive 1 min current traces were filtered at 2 kHz and acquired at 50 kHz sampling rate. In these conditions, spikes in the recorded cell appear as biphasic, small (20–200 pA peak-to-peak amplitude) current deflections (Fig. 1*C*). Recordings were judged to be stable when (i) the shape and amplitude of spikes was constant over time (Fig. 1*C*); and (ii) firing frequency was insensitive to changes in pipette holding potential. Stable recordings were routinely obtained for as long as 30–40 min (Fig. 1*C* and *D*). Giga-seal cell-attached recordings were not suitable for this study, because they often showed partial transition to the WC configuration after a few minutes, as signalled by abrupt changes in spike waveform and frequency.

### Whole-cell recordings

WC GoC recordings were performed with a potassium gluconate-based intracellular solution (KG) containing

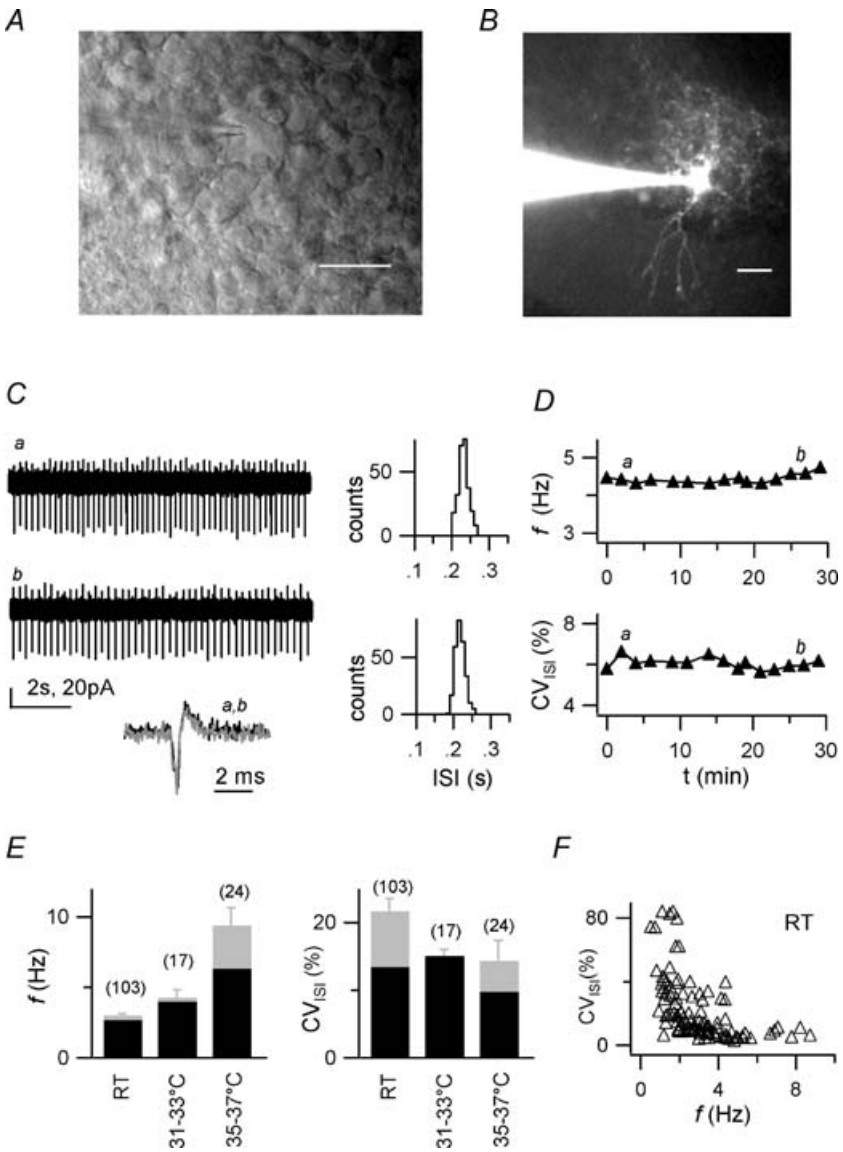


**Figure 1. Spontaneous firing of cerebellar Golgi cells in loose cell-attached recordings**
*A*, DIC-IR image of the surface of a cerebellar slice. A patch pipette is in contact with a GoC in the granular layer. Scale bar: 10 $\mu$m. *B*, fluorescence image of a GoC filled with Alexa Fluor 488. Note the apical dendrites extending in the molecular layer (lower part of image) and the extended plexiform axonal arborization in the granular layer (upper part). Scale bar: 20 $\mu$m *C*, left: loose cell-attached (LCA) current traces showing spontaneous single-spike firing at the beginning (upper trace, *a*) and at the end (lower trace, *b*) of a 30 min recording (RT). Biphasic downward and upward deflections represent spikes. Inset: single superimposed spikes from traces *a* and *b* shown at higher time resolution to illustrate constancy of spike waveform. Right, interspike interval (ISI) distributions from 1 min time windows ('1 min ISI distributions') including trace *a* (upper histogram; mean ISI and $CV_{ISI}$: 231 ms and 6.1%) and trace *b* (lower histogram; mean ISI and $CV_{ISI}$: 218 ms and 6.0%). *D*, time course of firing frequency *f* (top) and $CV_{ISI}$ (bottom) for the recording shown in *C*. Note the low variability, and stability of *f* and $CV_{ISI}$ over time. Labels indicate time position of traces *a* and *b* shown in *C*. *E*, summary of *f* (left) and $CV_{ISI}$ (right) statistics for a population of 103 cells at room temperature (RT), for 17 cells at 31–33°C and for 24 cells at 35–37°C. Grey bars: mean values ± S.E.M.; black bars: median values.
*F*, plot of $CV_{ISI}$ *vs* *f* for 103 cells studied at RT. Note the inverse correlation between $CV_{ISI}$ and *f* (see text). All recordings in *C*–*F* obtained in standard extracellular solution.

(mM): potassium gluconate 135 or 145, KCl 5, Hepes 10, EGTA 0.2, $MgCl_2$ 4.6, ATP-$Na_2$ 4, GTP-Na 0.4, pH 7.35 (supplemented with 100 $\mu$M Alexa Fluor 488 in a subset of recordings). The liquid junction potential ($E_{LJ}$) between the bath and pipette solution was measured according to Neher (1992), and was 10 mV. $E_{LJ}$ has been subtracted from membrane potential ($V_m$) measurements throughout the text. Pipettes had resistances of 3–4 MΩ and were coated with dental wax; seal resistance was 2–5 GΩ. Signals were filtered at 2–10 kHz and acquired at 10–50 kHz. Recordings were only accepted for analysis if the basal current, when holding cells in voltage clamp at −70 mV, was positive to −100 pA. Pipette series resistance ($R_s$) was $25 \pm 2$ MΩ ($n = 74$), and was constantly monitored during experiments; $R_s$ compensation was not used. In current-clamp recordings, $V_m$ measurements were corrected offline for errors introduced by $R_s$. An apparent input resistance was evaluated both in current-clamp and voltage-clamp conditions ($R_{CC}$ and $R_{VC}$), as follows. In the current-clamp mode, $R_{CC}$ was measured, in cells maintained in a subthreshold regime (−77/−67 mV), as the chord of the $V_m$–current relation obtained from 1 s-long negative current injections which decreased $V_m$ down to −84/−72 mV (control experiments), or down to −111/−123 mV (experiments with ZD 7288 application). In the voltage-clamp mode, $R_{VC}$ was measured from the current change at the end of 100 ms-long voltage-clamp steps from −70 to −80 mV (traces filtered at 10 kHz and acquired at 50 kHz). The input membrane capacitance $C_m$ was approximately measured by subtracting the time-integral of steady-state current from the time-integral of total current developing during the same voltage-clamp step and dividing by the voltage jump. $R_{VC}$ and $C_m$ measured immediately after break-in were $522 \pm 332$ MΩ (mean ± s.d.; median value: 425 MΩ ($n = 45$) and $146 \pm 73$ pF (mean ± s.d.; $n = 45$; see also Dieudonné, 1998). $R_{VC}$ gradually decreased during recordings ($-32 \pm 4$% in 15–25 min, $n = 11$ cells in control saline; see Fig. 3*C*). At the same time, cells were gradually depolarized, sometimes after an earlier hyperpolarizing phase. In a group of 14 cells (out of 26 analysed in detail) the membrane gradually hyperpolarized for several minutes after break-in (1–20 min; median 8 min), as seen from the change in current needed to maintain a $V_m$ value of −70 mV ($I_{-70}$); from $-27 \pm 4$ pA at < 1 min from break-in, to $-13 \pm 6$ pA at the end of the hyperpolarizing period; $n = 14$; $P = 0.0001$, Wilcoxon matched-pairs test; see Fig. 3*D*); this hyperpolarizing phase was followed by slow progressive spontaneous depolarization ($I_{-70}$ was $-33 \pm 16$ pA at 18–22 min after break-in, $n = 9$). In the remaining 12 cells, spontaneous depolarization was observed from the beginning of the WC recording. When averaging over both groups, $I_{-70}$ changed from $-22 \pm 6$ pA to $-41 \pm 8$ pA between 10 min and 20 min from break-in ($n = 21$; $P = 0.008$, Wilcoxon matched-pairs test).

### Drug application

All drugs were applied through the general bath perfusion, flowing at ∼1.5 ml min$^{-1}$, with a ∼1 min dead time before solution entrance in the bath. 4-Ethylphenylamino-1,2-dimethyl-6-methylaminopyrimidinium chloride (ZD 7288), D-(−)-2-amino-5-phosphonopentanoic acid (D-APV), 2,3-dioxo-6-nitro-1,2,3,4-tetrahydrobenzo[f]quinoxaline-7-sulphonamide disodium salt (NBQX), 6-imino-3-(4-methoxyphenyl)-1(6*H*)-pyridazinebutanoic acid hydrobromide (SR 95531), (3-aminopropyl)(diethoxymethyl)phosphinic acid (CGP35348) (all from Tocris) and strychnine (SIGMA) stocks were prepared in water. (*S*)-α-Methyl-4-carboxyphenylglycine ((*S*)-MCPG; Tocris) was dissolved at 10 mM in extracellular saline (glucose, $CaCl_2$ and $MgCl_2$ omitted). Apamin (Latoxan, Valence, France) stock was prepared in a Hepes-buffered saline (mM: NaCl 100, Hepes 20, pH 7.4 with NaOH). Tetrodotoxin (TTX; Latoxan) stocks were prepared in 0.1 M sodium citrate. *N*-(2-amino-4-(4-fluorobenzylamino)-phenyl) carbamic acid ethyl ester (retigabine) and 10,10-bis(4-pyridinylmethyl)-9(10*H*)-anthracenone (XE991) were kindly provided by Dr M. Taglialatela (University of Naples, Italy) and were dissolved in DMSO at 50 mM; a second XE991-dihydrochloride (Tocris) 10 mM stock solution was prepared in water, and no significant differences were observed between effects of the two stocks. All other chemicals were from Sigma-Aldrich.

### Data analysis

For analysis, we used self-written routines in the IGOR environment (Wavemetrics, Lake Oswego, OR, USA). In LCA recordings, firing frequency ($f$) and variability of the interspike interval (ISI) were evaluated from the mean ISI and the ISI coefficient of variation ($CV_{ISI}$). $CV_{ISI}$ was computed as the squared root of the ratio of ISI standard deviation to mean ISI. Each $f$ and $CV_{ISI}$ value was computed from an ISI sample collected over a time window of 1 min. LCA experiments were accepted for analysis of pharmacological effects on firing only when $f$ change in a > 5 min control period preceding application of drugs was ≤ 10% (Fig. 1). Values used for the statistics of $f$ and $CV_{ISI}$ in control conditions and in the presence of synaptic blockers (see Results) were measured 1–3 min after seal formation and 3–5 min after application of blockers in each experiment.

In current-clamp recordings, properties of the action potential (AP) waveform were evaluated from the mean waveform, obtained by aligning 10–30 APs at

their peak (traces acquired at 20–50 kHz sampling rate). Spike threshold ($V_{thr}$) was the $V_m$ value where $dV_m/dt$ exceeded 5 mV ms$^{-1}$. Spike amplitude was the peak-threshold difference. Spike half-width was the time interval separating two successive crossings of 50% of spike amplitude during the rising and repolarizing AP phases. $t_{10–90}$ was the time required for $V_m$ to rise from 10% to 90% of spike amplitude. Mean subthreshold $V_m$ was calculated from a 10–30 s trace, excluding values with $V_m > V_{thr}$. AHP trough was the minimum $V_m$ value in the subthreshold interspike period; AHP rise was the time interval separating threshold crossing during spike repolarization and attainment of the AHP trough. Sag amplitude was the difference between minimum and steady-state $V_m$ during a 1 s-long current step decreasing $V_m$ down to $-117.3 \pm 1.3$ mV (mean ± s.d.; range $-123$ to $-111$ mV; obtained with $-150$ to $-350$ pA; $n = 8$), either from a subthreshold regime ($-77/-67$ mV), or from the autorhythmic firing condition.

Statistics reported are mean ± standard error of the mean (s.e.m.) unless specified. Statistical non-parametric (for samples with $n > 5$) or parametric (for samples with $n = 5$) tests were performed using Instat (Graphpad Software, San Diego, CA, USA). Two-tailed $P$ values were used throughout.

## Results

### Spontaneous single-spike firing of cerebellar Golgi cells in loose cell-attached recordings

In this paper we report an electrophysiological investigation covering 237 GoCs (181 cells recorded at room temperature (RT) and 56 cells at 32–37°C) recorded in acute slices obtained from the rat cerebellum in the third postnatal week. GoCs were visually selected as cells presenting a large soma (> 10 $\mu$m diameter; Fig. 1*A*), located down to ~20 $\mu$m below the surface of the GL in lobules II–VIII. We took care to avoid cells displaying the characteristic brush of unipolar brush cells (Mugnaini & Floris, 1994), or cells adjacent to the Purkinje cell layer and displaying a bipolar, fusiform soma shape, typical of Lugaro cells (Lugaro, 1894). Recent studies suggested that some Lugaro cells display a non-fusiform, multipolar soma morphology and are found at different levels in the GL (Geurts *et al.* 2001; Lainé & Axelrad, 2002). Therefore, besides visual selection, a further criterion is needed for GoC identification. In slices, Lugaro cells are in a resting state, and shift to rhythmic firing upon serotonin application (Dieudonné & Dumoulin, 2000). In order to exclude Lugaro cells, we limited analysis to cells displaying single-spike rhythmic firing in standard extracellular saline. This condition was met, at RT, in 87% of the cells (103 out of 120) studied with LCA recordings and by 81% (78 out of 96) of the cells studied with WC recordings. In the latter case, the presence of single-spike rhythmic firing was assessed in the cell-attached configuration prior to break-in or immediately thereafter. When maintaining slices at more physiological temperatures (32–37°C), 80% of the visually selected large-soma interneurons (56 out of 70) displayed single-spike rhythmic firing. The remaining cells were either silent, with sporadic appearance of short spike sequences, or displayed bursting activity (not shown).

A subset of the visually selected cells subjected to WC recording (RT) was filled with the fluorescent dye Alexa Fluor 488 (100 $\mu$M). These cells displayed a dendritic arborization extending in both the granular and molecular layers. In 81% of cases (30/37 cells), the characteristic GoC axonal plexus with extended ramification into the GL (Golgi, 1883; Eccles *et al.* 1967) was observed (Fig. 1*B*). The remaining seven cells could have been GoCs with cut axon, or belonged to unrecognized different neuronal classes. Of the 30 cells endowed with a GoC-like axon, five were irregularly bursting or silent and were not analysed; as a consequence, the requirement for single-spike rhythmicity used in this study could have excluded a silent or bursting subpopulation of GoCs.

When recording with the LCA configuration (Fig. 1*C*), the firing frequency ($f$) of GoCs at RT was $3.0 \pm 0.2$ Hz (range 0.5–8.8 Hz, $n = 103$; Fig. 1*E*). In control conditions, firing continued for the entire length of recordings (up to 30–40 min) with minimal changes of frequency and precision (Fig. 1*C* and *D*). The interspike interval (ISI) variability was measured by the coefficient of variation of the ISI ($CV_{ISI}$). $CV_{ISI}$ median value at RT was 13.4% ($n = 103$; Fig. 1*E*), indicating that firing was highly regular in a large fraction of GoCs. $CV_{ISI}$ was inversely correlated to firing frequency, being larger for lower frequencies (Spearman correlation coefficient: $r = -0.6983$, $P < 0.0001$; Fig. 1*F*). Firing frequency increased with temperature (Fig. 1*E*), being $4.2 \pm 0.6$ Hz at 31–33°C (range 1.6–11.6 Hz, $n = 17$) and $9.3 \pm 1.3$ Hz at 35–37°C (range 2.6–21.6 Hz, $n = 24$; $P < 0.0001$, non-parametric ANOVA), while the $CV_{ISI}$ median value was relatively temperature insensitive, being 15% at 31–33°C and 9.7% at 35–37°C (Fig. 1*E*; $P = 0.152$, non-parametric ANOVA).

### Spontaneous single-spike firing is an autorhythmic activity

GoCs receive excitatory NMDA and AMPA/kainate glutamatergic synaptic inputs (Dieudonné, 1998; Bureau *et al.* 2000; Misra *et al.* 2000) as well as glycinergic and GABAergic inhibitory synaptic inputs (Dieudonné, 1995; Dieudonné & Dumoulin, 2000), which may be spontaneously activated by recurrent activity in the slice preparation. Therefore, the ability to generate spontaneous

rhythmic firing could depend on the activation of fast chemical synapses impinging onto GoCs. When addressing this issue in LCA recordings, we observed that firing was only slightly, although significantly, altered (Fig. 2*A* and *B*) upon bath application of a mixture of blockers of the above-mentioned ionotropic postsynaptic receptors ('synaptic blockers'; NBQX, 10 $\mu$M; D-APV, 25 $\mu$M; strychnine, 300 nM, and SR 95531 (gabazine), 30 $\mu$M). In fact, $f$ was $3.6 \pm 0.4$ Hz with synaptic blockers and $3.9 \pm 0.4$ Hz in control ($n = 20$ cells; $P = 0.024$, Wilcoxon matched-pairs test; Fig. 2*B*), with a blockers/control frequency ratio of $0.92 \pm 0.03$. The effect of synaptic blockers developed in 2–3 min (Fig. 2*A*). Firing precision was not significantly influenced ($CV_{ISI}$ in control: $11.9 \pm 2.0\%$, $CV_{ISI}$ with blockers: $10.9 \pm 1.8\%$, $n = 20$ cells; $P = 0.7285$, Wilcoxon matched-pairs test; Fig. 2*B*), and in no case was firing blocked. This result shows that spontaneous rhythmic firing in GoCs does not depend on phasic input from afferent synapses, but rather is generated by intrinsic excitable mechanisms.

Intrinsic excitability in the slice preparation might be increased by tonic depolarization which could force the cell into the firing regime. This could occur if, for example, accumulated glutamate or GABA were activating G-protein-coupled Glu (mGlu) and $GABA_B$ receptors, leading to modulation of relevant ionic currents. Specific expression in GoCs of mGluR2 (mGluR group II) and mGluR5/mGluR1 (mGluR group I) has been documented (Knoflach *et al.* 2001, and references therein), and a high density of $GABA_B$ receptors is found in the cerebellar cortex (Turgeon & Albin, 1993). We therefore studied the effect of inhibiting the activation of mGluRs (groups I and II) and $GABA_B$ receptors with bath application of the same mixture of 'synaptic blockers' as above, to which we added the non-selective mGluR group I/group II antagonist (*S*)-MCPG (500 $\mu$M), the $GABA_B$ antagonist CGP 35348 (100 $\mu$M), or both. In all cases, rhythmic firing (monitored at 35–37°C) continued after application of drugs with no significant changes in frequency or precision (after 10 min in CGP 35348: $f = 6.3 \pm 1.3$ Hz, *vs* $5.9 \pm 1.5$ Hz

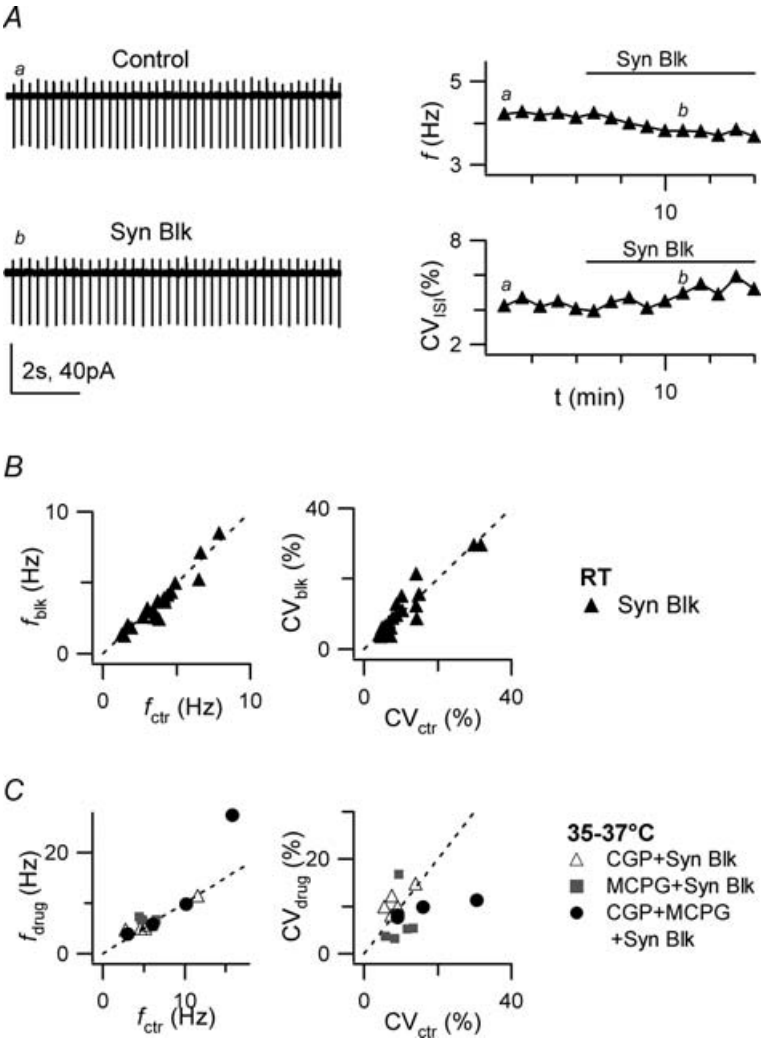


**Figure 2. Rhythmic firing is resistant to block of fast synaptic inputs and mGluR and $GABA_B$ receptors**
Effect of synaptic input block with NBQX (10 $\mu$M), D-APV (25 $\mu$M), SR 95531 (30 $\mu$M) and strychnine (300 nM) ('synaptic blockers') and with mGluR group I/II and $GABA_B$ receptors antagonists. *A*, left: LCA traces showing firing activity (at RT) before ('Control') and after applying synaptic blockers for 6 min ('Syn Blk'). Right: time course of firing frequency $f$ (upper plot) and $CV_{ISI}$ (lower plot) for the same experiment. The horizontal bars indicate time of drug application; labels indicate time position of traces *a* and *b* shown on the left. Note that firing frequency and $CV_{ISI}$ are only marginally affected. *B*, plot of firing frequency and $CV_{ISI}$ in the presence of synaptic blockers ($f_{blk}$, $CV_{blk}$), *vs* corresponding values before blockers ($f_{ctr}$, $CV_{ctr}$) for 20 cells (RT). *C*, plot of firing frequency (at 35–37°C) and $CV_{ISI}$ ($f_{drug}$, $CV_{drug}$) in the presence of a mixture of synaptic blockers and CGP 35348 (100 $\mu$M; △; 5 cells) (*S*)-MCPG (0.5 mM; ■; 5 cells) and CGP 35348 + (*S*)-MCPG (●; 4 cells), *vs* corresponding values in control ($f_{ctr}$, $CV_{ctr}$). Firing frequency and $CV_{ISI}$ are non-significantly affected by drug application in all cases.

in control, $n = 5$, $P = 0.433$; $CV_{ISI} = 10.9 \pm 1.2\%$, *vs* $8.8 \pm 1.4\%$, $n = 5$, $P = 0.089$; after 6–8 min in (*S*)-MCPG: $f = 6.5 \pm 0.3$ Hz, *vs* $5.3 \pm 0.4$ Hz in control, $n = 5$, $P = 0.1546$; $CV_{ISI} = 6.8 \pm 2.5\%$, *vs* $9.7 \pm 1.3\%$, $n = 5$; $P = 0.3456$; after 5–8 min in (*S*)-MCPG + CGP 35348: $f = 11.7 \pm 5.3$ Hz, *vs* $8.8 \pm 2.8$ Hz in control, $n = 4$, $P = 0.386$; $CV_{ISI} = 9.2 \pm 0.8\%$, *vs* $16.2 \pm 5.1\%$, $n = 4$, $P = 0.202$; paired *t* test; Fig. 2*C*). In experiments conducted in the absence of synaptic blockers, (*S*)-MCPG (500 $\mu$M) application inhibited the pause in GoC spontaneous firing following an evoked train of spikes triggered by extracellular stimulation in the cerebellar molecular layer (not shown); such decrease in GoC excitability after intense parallel fibre release has been studied by Watanabe & Nakanishi (2003) and found to depend on mGluR2 activation. CGP 35348 (100 $\mu$M) application was effective in modulating the constitutive inward rectifier $K^+$ current of granule cells in parallel slice experiments in our laboratory (P. Rossi *et al.*, 2006). These observations confirm that (*S*)-MCPG and CGP 35348 applications were effective in our experiments. In conclusion, we found that block of group I/group II mGluRs and $GABA_B$ receptors does not block rhythmic firing in GoCs, and this rules out the possibility that firing is due to depolarization arising after activation of these receptors by ambient Glu and GABA present in the slice. These data further support the notion that GoCs are endowed with intrinsic mechanisms to sustain autorhythmic, pacemaker activity.

The rest of this work is devoted to uncovering the ionic mechanisms generating the pacemaker cycle in autorhythmic GoCs. We performed all subsequent experiments at RT in the presence of blockers of fast synaptic transmission ('synaptic blockers', as above). We investigated the presence and role of several candidate currents including subthreshold $Na^+$ currents, the hyperpolarization-activated cationic current ($I_h$), the M-type $K^+$ current ($I_M$) and the apamin-sensitive $K^+$ current ($I_{apa}$).

### Whole-cell recordings from Golgi cells

GoCs were further studied with the current-clamp WC configuration. When breaking into GoCs using potassium gluconate-based pipette solutions, spontaneous firing continued in 32 of 41 cells. In these cells, spike waveform exhibited rapid rise and decay (Table 1; Fig. 3*A*). The subthreshold interspike trajectory ('pacemaker range'; Table 1 and Fig. 3*A*) showed a pronounced AHP and spanned from $\sim -75$ mV (AHP trough) to $\sim -55$ mV (spike threshold). Comparison of firing frequency before and 1–2 min after membrane rupture (no injected current) showed a significant increase (gigaseal cell-attached, *f*: $3.2 \pm 0.3$ Hz; whole-cell, *f*: $4.6 \pm 0.6$ Hz; $n = 32$ cells; $P = 0.048$, Wilcoxon matched-pairs test). In 8 out of 16 cells (50%) in which spontaneous firing was continuously monitored, *f* decreased, and eventually firing stopped within a few minutes after membrane rupture (Fig. 3*B*). In all cases, the apparent input resistance (measured in voltage clamp, $R_{VC}$; see Methods and Fig. 3*C*) and the current needed to maintain $V_m$ at $-70$ mV (measured in current clamp, $I_{-70}$; see Methods and Fig. 3*D*) showed progressive changes after break-in. These effects, which are possibly linked to cytoplasmic dialysis and/or increasing leak conductance through the seal, are likely to perturb the delicate balance of small ionic currents active in the subthreshold region. Therefore, in order to study the impact of pharmacological block of ionic currents on spontaneous firing, we took advantage of the LCA configuration, which, as reported above, permits long stable recordings of firing activity. WC recordings provided useful information on some functional parameters which were stable enough during several tens of minutes. These were, in current-clamp recordings, the firing frequency-to-injected current (*f–I*) relationship (see below and Fig. 3*F*) and the extent of inward rectification at negative potentials (Fig. 5); in voltage-clamp recordings, the amplitude of subthreshold persistent $Na^+$ current (Fig. 4).

Upon injection of 1 s-long positive current steps of increasing amplitude (Fig. 3*E* and *G*), the instantaneous firing frequency at the onset of the response ($f_{in}$) followed linearly the input current, reaching values up to $\sim$200 Hz ($n = 6$ cells; holding current 0 pA; 3–9 Hz basal firing frequency; Fig. 3*G*). Spike frequency adaptation at the end of depolarizing steps (measured as $1 - (f_{1s}/f_{in})$, where $f_{1s}$ is instantaneous frequency estimated at the end of the step) was modest ($11 \pm 3\%$) for $f_{in}$ in the 7–35 Hz range, and increased to $74 \pm 12\%$ for $f_{in}$ in the 200–210 Hz range (Fig. 3*H*; see also Fig. 3 in Dieudonné, 1998). Thus GoCs can generate repetitive firing upon a large range of depolarizing input intensities.

**Table 1. Mean properties of AP and interspike interval in GoCs**

| | Mean ± S.E.M. ($n = 6$) |
|---|---|
| Spike peak | $21.8 \pm 3.6$ mV |
| Spike threshold | $-55.3 \pm 1.0$ mV |
| Spike half-width | $1.22 \pm 0.08$ ms |
| $t_{10–90}$ | $440 \pm 28$ $\mu$s |
| Mean *V* subthreshold | $-67.9 \pm 1.0$ mV |
| AHP trough | $-74.9 \pm 1.5$ mV |
| AHP rise | $37 \pm 6$ ms |

All parameters were measured during the pacemaker cycle in six morphologically identified GoCs (GoC-like axon present) firing at 2.5–3.6 Hz in current-clamp recordings (RT; holding current in the range $-20$ to $+10$ pA). In this frequency range, there was no correlation between measured AP parameters and frequency. $t_{10–90}$, 10–90% spike rise time. See Methods for details.

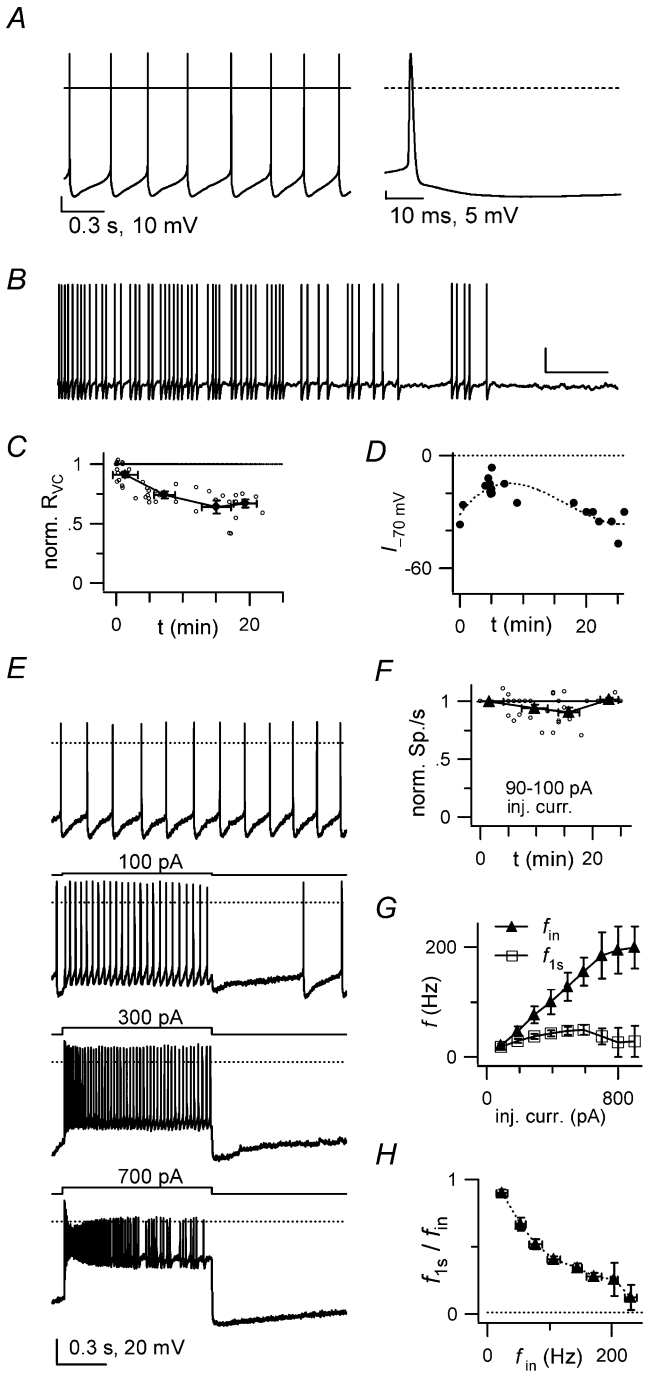


**Figure 3. Whole-cell current-clamp GoC recordings**
*A*, left: autorhythmic firing (3.7 Hz) in a GoC with synaptic blockers present. Holding current ($I_{hold}$): 0 pA. Note the pronounced after-hyperpolarization after each spike. Horizontal bar: 0 mV level. Right: a spike from the left trace, displayed with higher time resolution. *B*, a longer voltage trace from another cell ($I_{hold}$ 0 pA). Note the decrease in autorhythmic firing frequency occurring in the course of a few tens of seconds. Scale bars: 5 s, 20 mV. *C*, summary of apparent input resistance ($R_{VC}$) values, measured from voltage-clamp steps between −70 and −80 mV (see Methods), collected from 11 cells and plotted *vs* experimental time. Values are normalized to $R_{VC}$ in the first minute after break-in. *D*, time plot of the current injection through the patch pipette needed to maintain $V_m$ at ∼−70 mV ($I_{-70}$) in a single cell. Note the initial $I_{-70}$ increase, indicating membrane hyperpolarization, followed, after > 8 min, by progressive $I_{-70}$ decrease, indicating subsequent depolarization. This behaviour was noticed in ∼50% of the cells. *E*, whole-cell (WC) current-clamp voltage traces showing responses of a GoC to 1 s-long step current injections of increasing amplitude, as indicated above traces. Top trace: $I_{hold}$ 0 pA, autorhythmic firing, 6.6 Hz. Bottom two traces: note spike frequency adaptation for large current input. Dotted bar: 0 mV level. *F*, number of spikes during a 1 s-long step current injection of 90–100 pA ($N_{90–100}$), as a function of time from break-in, normalized to the value in the first minute (54 data points from 9 cells; small open circles). Average $N_{90–100}$ (filled symbols) decreases from 12.6 ± 1.0 spikes to 12.3 ± 1.0 spikes in the first 10–15 min (−2.9 ± 4.1%). *G*, frequency–current (*f–I*) relationships for six cells studied as in *E*. $f_{in}$ (filled symbols) and $f_{1s}$ (open symbols) are plotted *vs* injected current (inj. curr.). $I_{hold}$ 0 pA; autorhythmic firing frequency: 3.2–7.1 Hz. *H*, ratio of $f_{1s}$ to $f_{in}$, plotted *vs* $f_{in}$, for the same six cells as in *G*. Note the progressive spike frequency adaptation with larger inputs.

At the end of discharge in response to depolarizing pulses, GoCs showed a marked AHP which delayed the re-establishment of pacemaker activity (Fig. 3*E*). The AHP depth and duration increased with stimulation intensity.

### Subthreshold $Na^+$ current

$Na^+$ currents active in the subthreshold range ($I_{Na,sub}$) have been implicated in the generation and regulation of pacemaker activity in several neuronal types (see Introduction). The effects of TTX block of subthreshold and suprathreshold $Na^+$ currents cannot be separated while observing occurrence of spikes with LCA recordings; therefore we could not directly verify the functional effect of $I_{Na,sub}$ in spontaneous firing. Indirect information can nevertheless be obtained by measurement of $I_{Na,sub}$ during somatic GoC voltage clamp in a restricted voltage range (−70 to −60 mV), where artefacts due to axial current flow arising from imperfect space clamp and to series resistance are minimized (White *et al.* 1995). We examined responses to 2 s-long voltage steps from a holding potential of −70 mV up to −60 mV before and after TTX application (500 nM; Fig. 4*A*). Subtraction of average traces obtained from control periods and after reaching steady-state TTX block revealed a TTX-sensitive steady inward current (Fig. 4*A* and *B*), activating positive to −70 mV (Fig. 4*C*), which had an amplitude of −23 ± 5 pA at the end of a step to −60 mV ($n = 5$; Fig. 4*D*). This indicates that $I_{Na,sub}$ is active in GoCs at voltages positive to −70 mV, and therefore should take part in the slow pacemaker depolarization leading to spike threshold. Moreover, the current remaining after TTX block at command voltages positive to −60 mV was outward at all times during the step ($n = 4$ out of 5 cells); given that spike threshold in GoCs is ∼−55 mV (Table 1), this suggests that the TTX-sensitive current is necessary to drive GoC pacemaking.

### Hyperpolarization-activated current ($I_h$)

A $Cs^+$-sensitive inward rectification of GoC membrane current at negative voltages has been shown in the rat by Dieudonné (1998) and in the turtle by Midtgaard (1992), suggesting the presence of an $I_h$ current. To confirm the presence of inwardly rectifying currents in GoCs in current-clamp recordings, we examined responses to 1 s-long negative current steps from cells maintained in a subthreshold regime (−77/−67 mV) by means of negative steady current injection. At 7–21 min from break-in, responses showed a characteristic, stable, slowly developing voltage sag, suggesting the slow opening of $I_h$ channels (Fig. 5*A*). Consistently, at the end of hyperpolarizing current injection, a transient after-depolarization indicated the delayed deactivation of $I_h$ channels activated at negative potential (Fig. 5*A*). Return from hyperpolarization into the firing region was often associated with a short spike burst (not shown).

GoC apparent input resistance ($R_{CC}$; see Methods) significantly decreased during the step (at the time of $V_m$ minimum: $340 \pm 44$ MΩ; after 1 s: $244 \pm 32$ MΩ; $n = 8$ cells; Fig. 5*B*). The voltage sag amplitude, for negative current steps hyperpolarizing $V_m$ down to $-117 \pm 1$ mV, was $11.4 \pm 1.9$ mV ($n = 8$; Fig. 5*A*). In six cells, inward rectification was largely reduced by perfusing slices with the bradicardic agent ZD 7288 (20 $\mu$M), a potent ($IC_{50}$ for $I_h$ block in brain slices: 10.5 $\mu$M, Gasparini & DiFrancesco, 1997; 2.3 $\mu$M, Neuhoff *et al.* 2002) and selective $I_h$ blocker (e.g. Dickson *et al.* 2000; but see Do & Bean, 2003) (Fig. 5*C*). Peak and steady-state $R_{CC}$ were increased by $44 \pm 7\%$ and $81 \pm 17\%$ by the drug (from $266 \pm 23$ to $379 \pm 33$ MΩ, $P = 0.031$, peak $R_{CC}$; from $193 \pm 26$ to $333 \pm 32$ MΩ, $P = 0.031$, steady-state $R_{CC}$; Wilcoxon matched-pairs tests; $n = 6$ cells), indicating the presence of a ZD 7288-blocked current which developed along the step (Fig. 5*D*). The $V_m$ sag decreased by $51 \pm 5\%$ after 8–12 min drug application (from $12.9 \pm 3.0$ mV to $6.1 \pm 1.4$ mV, $n = 6$, $P = 0.031$, Wilcoxon matched-pairs test; Fig. 5*C*). These data indicate that slow inward rectification was sustained by activation of $I_h$, and further confirm that a robust $I_h$ current is present in GoCs.

We investigated the role of $I_h$ in GoC pacemaking by studying firing properties in LCA recordings before and after slice perfusion with ZD 7288 (20 $\mu$M). The onset of the ZD 7288 effect on firing frequency was slow, starting 5–12 min after application, and led to slow progressive $f$ decrease (Fig. 6*A* and *B*; $n = 7$ cells): 10 min after the start of the ZD 7288 effect, $f$ had decreased on average by ∼59%, from $3.9 \pm 0.8$ Hz (range 2.7–8.5 Hz) in control to $1.4 \pm 0.2$ Hz (range 0.75–2.1 Hz) ($P = 0.016$, Wilcoxon matched-pairs test; Fig. 6*C*). In parallel with frequency,

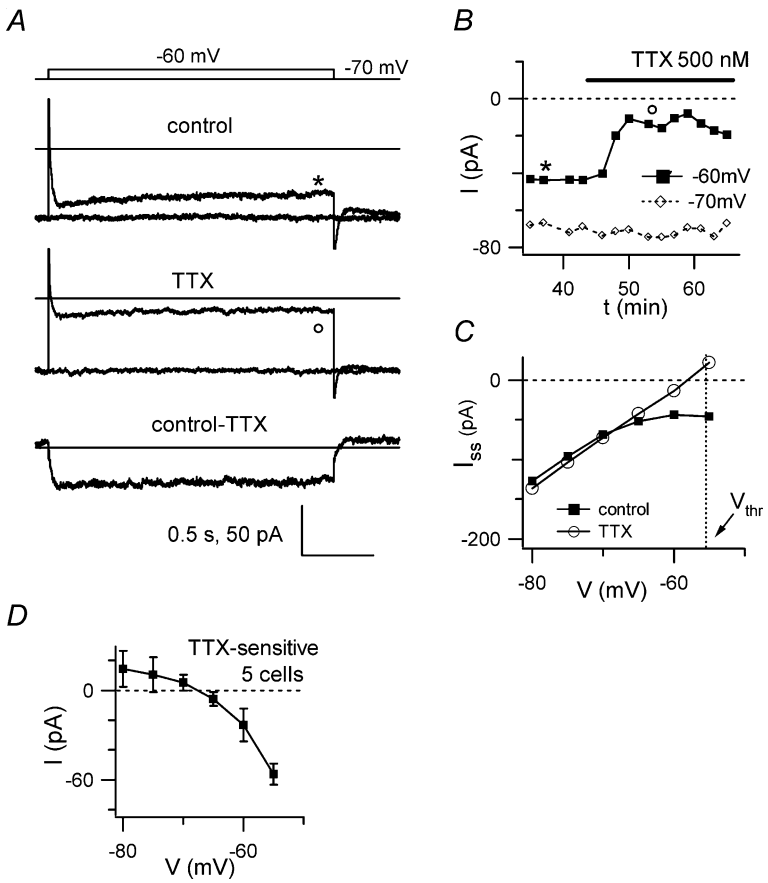


**Figure 4. TTX effect on subthreshold membrane current**
In voltage-clamp experiments exploring a small subthreshold voltage range TTX (500 nM) abolishes a steady inward component. *A*, current traces in response to voltage-clamp steps from −70 mV (holding potential) to −60 mV, before (top) and after TTX application (middle); the lower trace is the TTX-sensitive current, obtained from subtraction of the middle from the upper trace. Horizontal lines indicate the zero current level. The voltage protocol is shown above traces. *B*, for the same cell, plot of steady-state current at −70 mV (open symbols) and at the end of a 2 s step from −70 to −60 mV (filled symbols) *vs* experimental time. Cells used for these experiments reached a stable current baseline at −70 mV after ∼20–30 min from break-in. Bar indicates the period of TTX application. Note the TTX-induced decrease of inward current at −60 mV. Markers indicate the time of current traces reported in *A*. *C*, current–voltage relation in the −80/−55 mV range for the cell in *A*, before (■) and after (○) TTX. The vertical dashed line reports the average value of GoC spike threshold ($V_{thr}$) for reference, to show that TTX-resistant current at threshold is positive. *D*, average TTX-sensitive current *vs* voltage in the −80/−55 mV range (5 cells). Positive current at voltages ≤ −70 mV might be accounted for by space-clamp errors (White *et al*. 1995).

firing precision also decreased (Fig. 6*A* and *B*), with $CV_{ISI}$ increasing from $10.4 \pm 2.6\%$ to $26.4 \pm 7.6\%$ (control *vs* ZD 7288; $P = 0.016$, Wilcoxon matched-pairs test; 10 min after application; Fig. 6*C*). This 'early' effect was followed, in three of seven cells, by a progressive clustering of spikes, appearing 10–20 min after drug application and sometimes ending in a clear bursting behaviour (not shown). The initial frequency decrease and the associated CV increase can be explained by a decrease of an inward current contributing to subthreshold pacemaker depolarization; it is therefore consistent with $I_h$ block as the mechanism mediating the early effect of ZD 7288.

A further manipulation producing block of $I_h$ is application of extracellular $Cs^+$ ions (reviewed in Pape, 1996), also known to block a variety of $K^+$ conductances (reviewed in Garcia *et al.*, 1997). Application of CsCl (2 mM) in GoC LCA recordings had opposite effects to ZD 7288, with a significant acceleration of firing ($n = 3$; not shown), suggesting that the main effect of $Cs^+$ was block of outward $K^+$ conductances, leading to moderate cell depolarization and subsequent frequency increase (Do & Bean, 2003).

Do & Bean (2003) reported inconsistent effects of ZD 7288 on firing in subthalamic nucleus neurons,

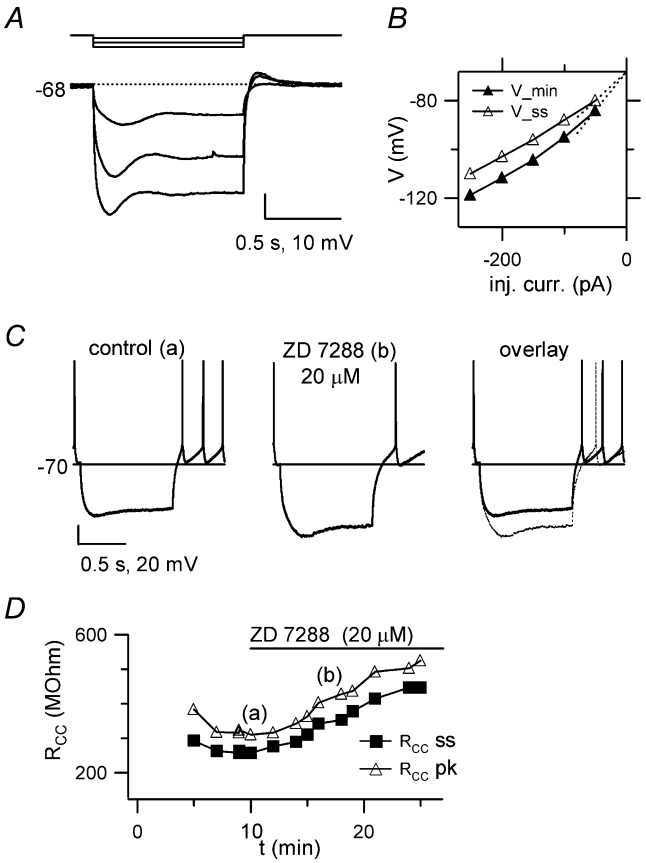


**Figure 5. ZD 7288-sensitive inward rectification in GoCs**
A Voltage responses to 1 s-long negative current injections (−50, −150 and −250 pA). The cell is hyperpolarized to −68 mV with −50 pA steady injection. Note the inward rectification during the step and rebound excitation after step termination. *B*. minimum (▲; $V_{min}$) and steady-state (△; $V_{ss}$) voltage during negative step injections, plotted *vs* injected current, for the cell in *A*, to further illustrate slow inward rectification at negative potentials. *C*, voltage responses to 1 s-long −150 pA current injection, before and 10 min after ZD 7288 (20 μM) application. Holding current: 0 pA, autorhythmic firing: 3.7 Hz (control trace), 2.5 Hz (ZD 7288 trace). *D*, apparent input resistance $R_{CC}$ *vs* experimental time, for the cell in *C*. $R_{CC}$ is calculated from the voltage displacement from −70 mV generated by a −150 pA injection, measured at the voltage minimum ($R_{CC}$ pk, △) or at the end of the step ($R_{CC}$ ss; ■). The bar marks the period of ZD 7288 application. Note the $R_{CC}$ decrease in the control period, and the $R_{CC}$ increase induced by the drug.

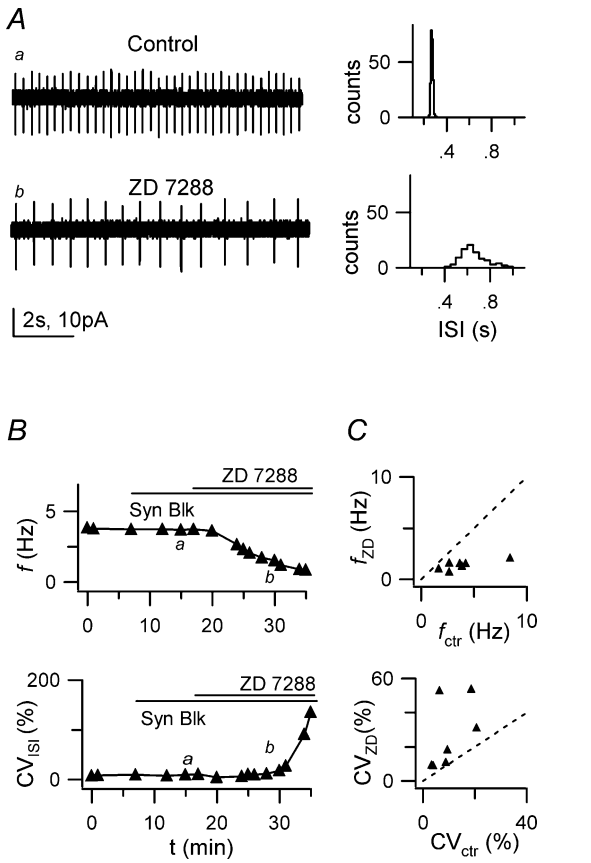


**Figure 6. Block of $I_h$ with ZD 7288 reduces firing frequency and precision**
*A*, left: LCA traces before (*a*) and after (*b*) bath application of 20 μM ZD 7288, in the presence of synaptic blockers. Right, 1 min ISI distributions for traces on the left. Mean ISI and $CV_{ISI}$: 270 ms and distribution 3.6% (upper histogram) and 653 ms and 16.4% (lower histogram).
*B*, time course of *f* (upper plot) and $CV_{ISI}$ (lower plot) for the recording shown in *A*, indicating a large *f* decrease and $CV_{ISI}$ increase during drug application. Horizontal bars indicate times of synaptic blockers and ZD 7288 application; labels indicate time position of traces *a* and *b* shown in *A*. *C*, plot of *f* (top) and $CV_{ISI}$ (bottom) in the presence of ZD 7288 ($f_{ZD}$, $CV_{ZD}$), *vs* respective values in control ($f_{ctr}$, $CV_{ctr}$), for 7 cells.

proposed to arise from non-specific blocking effects. They show that ZD 7288 (10 $\mu$M) blocks an outward, hyperpolarizing current developing while the membrane potential trajectory spans the subthreshold pacemaker range; this is paralleled, in current-clamp recordings, by membrane depolarization, firing frequency increase and, in some cells, by 'depolarization block' of firing. In all GoC LCA recordings, $f$ did gradually decrease over 10–20 min during ZD 7288 application, without ever accelerating or stopping. This is in contrast to the effects expected from progressive depolarization that should lead to $f$ increase and eventually to abrupt firing arrest, thus ruling out the possibility that the effect of ZD 7288 on GoC firing is caused by block of outward currents. In conclusion, our data show that a ZD 7288-sensitive $I_h$ current has an important role in sustaining GoC pacemaker activity.

### Retigabine-sensitive M-type $K^+$ currents

Neuronal $K^+$ currents active in the subthreshold voltage range generate hyperpolarizing current counteracting slow pacemaker depolarization and contributing to the determination of the interspike interval duration. A number of functional $K^+$ current types may in principle contribute to subthreshold repolarizing current. Besides the delayed-rectifier-type and BK-type $Ca^{2+}$- and voltage-dependent $K^+$ currents, which activate during or immediately following the spike and deactivate fast after repolarization, candidate $K^+$ currents include slowly activating M-like, transient outward A-type and SK-type $Ca^{2+}$-dependent $K^+$ currents, together with voltage-independent 'leak' channels. We initiate the analysis of $K^+$ currents contributing to the determination of the pacemaker rhythm in GoCs by focusing on retigabine-sensitive M-like $K^+$ currents and apamin-sensitive SK-type $Ca^{2+}$-dependent $K^+$ currents.

Among the available pharmacological tools for the study of the M-type $K^+$ current $I_M$ is the cognition-enhancing drug XE991, which blocks heterologously expressed neuronal KCNQ channels (KCNQ2–5) with variable potency depending on the specific subunit combination (Wang *et al.* 1998; Robbins, 2001) and is a potent $I_M$ blocker in intact neurons ($IC_{50} < 1$ $\mu$M; Wang *et al.* 1998; Oliver *et al.* 2003; Passmore *et al.* 2003; Romero *et al.* 2004). The anticonvulsant drug retigabine increases $I_M$ in heterologously expressed channels formed with KCNQ2–5 subunits (Main *et al.* 2000; Rundfeldt & Netzer, 2000; Tatulian *et al.* 2001; Wickenden *et al.* 2001) and increases $I_M$ in intact cells (Wickenden *et al.* 2000; Tatulian *et al.* 2001).

In order to gain information on the presence of functional KCNQ channels in GoCs, we studied the effect of bath perfusion of retigabine on cellular responses recorded during current-clamp whole-cell experiments. We injected 1 s-long depolarizing current steps in cells steadily hyperpolarized to −70 mV by current injection. Application of retigabine (5 $\mu$M) led, in a few minutes, to a clear excitability decrease, as measured from the decreased number of spikes evoked by a fixed-amplitude step. With steps of 90 or 100 pA, this number ($N_{90-100}$) was 12.1 ± 1.6 in control, and 6.2 ± 2.6 after 7–17 min in retigabine, corresponding to a −52 ± 16% decrease ($n = 5$; Fig. 7*A*–*C*). The decrease in $N_{90-100}$ after retigabine was significantly larger ($P = 0.002$, Mann-Whitney test) than spontaneous rundown in comparable time windows of control recordings (see Fig. 3*F*, legend). These results show that retigabine depresses cell excitability, and this is likely to be mediated by recruitment of functional KCNQ channels.

Retigabine is known to displace KCNQ channel activation towards negative potentials (Main *et al.* 2000; Wickenden *et al.* 2000, 2001; Tatulian *et al.* 2001) producing increased channel opening in the just-threshold range. In cells hyperpolarized to −70 mV by steady current injection, retigabine should therefore produce a hyperpolarizing shift and an accompanying input resistance decrease (e.g. Yue & Yaari, 2004; Gu *et al.* 2005). In our whole-cell experiments, the current needed to maintain $V_m$ at −70 mV ($I_{-70}$) became less negative after retigabine (3 cells), or remained nearly constant (2 cells). On average, $I_{-70}$ was −28 ± 8.5 pA in control at ∼10 min from break-in, and −17 ± 14.5 pA after 7–17 min in retigabine, i.e. 7–17 min later ($n = 5$). This $I_{-70}$ change is significantly different ($P = 0.029$, Mann-Whitney test) from the change observed in the same time window in control recordings, where $I_{-70}$ became more negative with time (see Methods and Fig. 3*D*). These observations are thus compatible with a hyperpolarizing effect of retigabine. The apparent input resistance measured in voltage clamp in the −70/−80 mV range decreased during recordings, before and after retigabine application (not shown), in a way similar to that observed in control whole-cell recordings (Fig. 3*C*), suggesting that the membrane conductance increase associated with the WC configuration masks the increase due to enhanced retigabine-mediated opening of KCNQ channels.

To investigate the role of KCNQ channels in GoC autorhythmic activity, we sought a selective antagonist rather than an agonist. We monitored firing properties in LCA recordings during bath application of XE991 (5 $\mu$M). After 10 min of continuous application, firing frequency $f$ and $CV_{ISI}$ were not significantly different from control (mean $f$ in control: 3.21 ± 0.73 Hz; after XE991: 3.31 ± 0.81 Hz; $n = 5$ cells; $P = 0.589$; mean $CV_{ISI}$ in control: 12 ± 5%; after XE991: 10 ± 4%; $n = 5$ cells; $P = 0.125$; paired $t$ tests; Fig. 8); further drug application for 5–10 min gave similar results (not shown). Two different XE991 stock solutions were used for this purpose (see Methods), with indistinguishable results. Therefore, we have no evidence

for a contribution of XE991-sensitive KCNQ channels to the regulation of pacemaker activity in GoCs.

In conclusion, our results suggest the functional presence in GoCs of a retigabine-sensitive M-like current. Due to low activation threshold and lack of inactivation, an M-like current would be expected to be active in the pacemaker range. Our experiments suggest that the retigabine-sensitive M-like current in GoCs is either XE991 insensitive, or, alternatively, it produces a small, non-relevant contribution in the pacemaker range (see Discussion).

### Apamin-sensitive $Ca^{2+}$-dependent $K^+$ currents

In several neuronal types, apamin-sensitive SK channel-mediated $Ca^{2+}$-dependent $K^+$ currents, $I_{apa}$, are involved in the generation of the AHP that develops after a single spike in the 10–100 ms time range (single-spike AHP or mAHP; reviewed in Stocker, 2004). To verify the presence of functional SK-type channels in GoCs, we studied the effect of the specific blocker apamin (50 nM; reported $IC_{50}$ for SK3 channels is 0.6–4 nM; reviewed in Stocker, 2004) on the single-spike AHP in whole-cell current-clamp recordings. After 2–4 min bath application, apamin decreased the AHP trough observed in spontaneously firing cells ($n = 5$; control: $-68.8 \pm 2.6$ mV; after 2–4 min in apamin: $-63.6 \pm 2.9$ mV; $P = 0.026$, paired $t$ test; Fig. 9*A*), indicating that $I_{apa}$ was contributing to the generation of the AHP. A clear apamin-induced decrease of the single-spike AHP amplitude was also observed in cells maintained at $-70$ mV with negative current injection and briefly (0.5 ms) stimulated with just-threshold current steps to evoke single spikes (not shown).

The effects of SK channel block on pacemaker activity were assessed using bath application of 50 nM apamin during LCA recordings. In cells displaying a basal firing frequency $> 2$ Hz, apamin perfusion induced a marked increase of ISI variability (Fig. 9*B–D*): $CV_{ISI}$ rose from $7.1 \pm 1.8\%$ (1 min before drug application) to $21.1 \pm 9.6\%$ (4–6 min after bath application), with a $3.1 \pm 0.8$-fold increase ($n = 5$; $P = 0.031$; paired $t$ test). Conversely, in two cells with low basal frequency (1.5 and 1.4 Hz) and large ISI variability, $CV_{ISI}$ was not significantly affected after apamin perfusion (0.2-fold

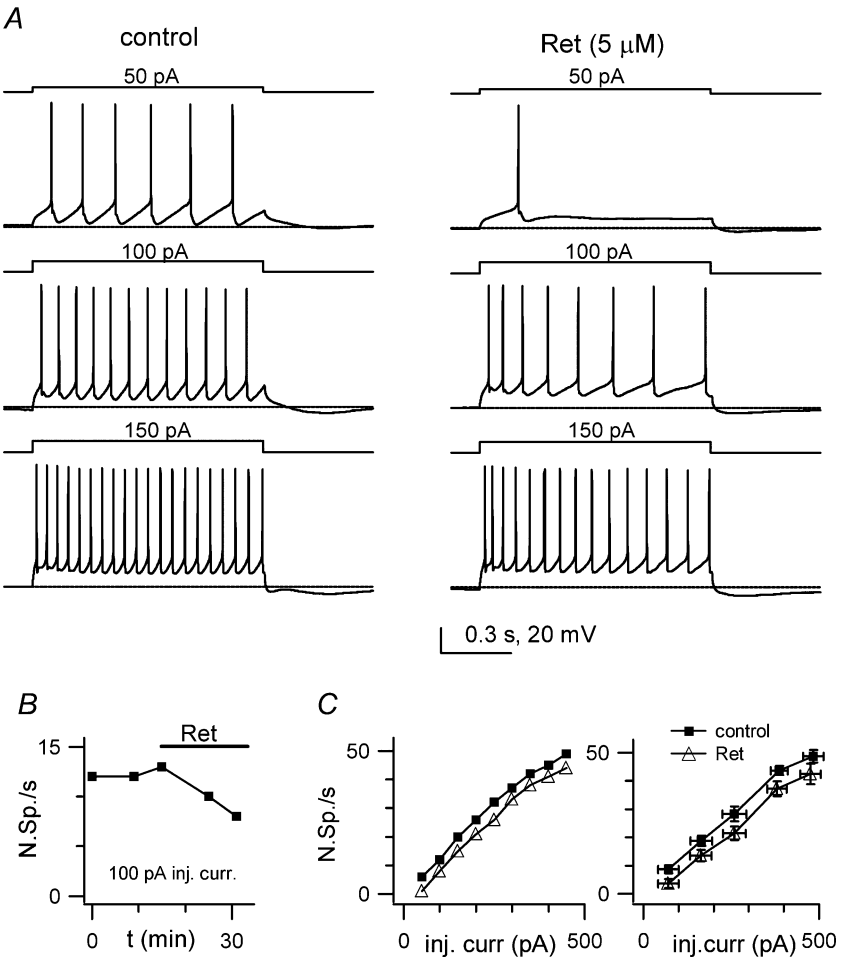


**Figure 7. The M-type current agonist retigabine decreases cell excitability**
*A*, voltage traces from a current-clamp WC recording showing responses of a GoC to 1 s-long step current injections of increasing amplitude (indicated above traces), in control (left) and 15 min after 5 $\mu$M retigabine application ('Ret'; right). Horizontal bars: $-70$ mV level. Note decreased spike numbers after drug for all step amplitudes *B*, number of spikes during a 1 s-long, 100 pA step current injection, as a function of time from break-in, for the experiment in *A*. The bar indicates retigabine application. *C*, number of spikes during a 1 s-long step current injection as a function of current amplitude, before (■) and 15 min after retigabine application (△). Left plot is for the same cell as above, right plot is a summary for 5 cells.

increase and 0.4-fold decrease). In spite of the large effect of apamin on firing precision, the effect on average firing frequency was not significant (control $f$: $3.0 \pm 0.4$ Hz, $f$ after 4–6 min in apamin: $2.9 \pm 0.5$ Hz, $P = 0.808$, paired $t$ test; $n = 7$). In conclusion, these results demonstrate that, in cerebellar GoCs, apamin-sensitive SK channels have an important role in determining the precision of the pacemaker mechanism.

## Discussion

Our investigation shows that Golgi cells in the rat cerebellum sustain spontaneous low-frequency rhythmic firing in the absence of phasic input. Firing continued after blocking the known GoC synaptic ionotropic receptors, namely glutamatergic receptors of the NMDA and non-NMDA types (Dieudonné, 1998; Bureau *et al.* 2000; Misra *et al.* 2000) and glycine and $GABA_A$ receptors (Dieudonné, 1995; Dieudonné & Dumoulin, 2000). We thus conclude that GoC firing is sustained by an intrinsic pacemaker mechanism, i.e. an appropriate set of membrane channels allowing the generation of rhythmic firing.

It should be noted that some neurons *in vivo* can switch between non-pacemaker and pacemaker properties in relation to behavioural requirements, as reported for neurons in the mammalian respiratory network, hypothalamus and basal ganglia and for crustacean neurons (reviewed in Ramirez *et al.* 2004; Surmeier *et al.* 2005). Neuromodulators play an important part in the induction, enhancement and suppression of pacemaker properties: through multiple channel modulations, excitability is increased or decreased, pushing a cell into the firing regime or away from it. Relevant neuromodulatory effects may also occur in slices in relation to accumulation or depletion of transmitters. However, GoC firing in our experiments was resistant to block of group I/group II mGluRs and $GABA_B$ receptors, showing that periodic activity was not due to depolarization arising after activation of these receptors by ambient glutamate and GABA. While there

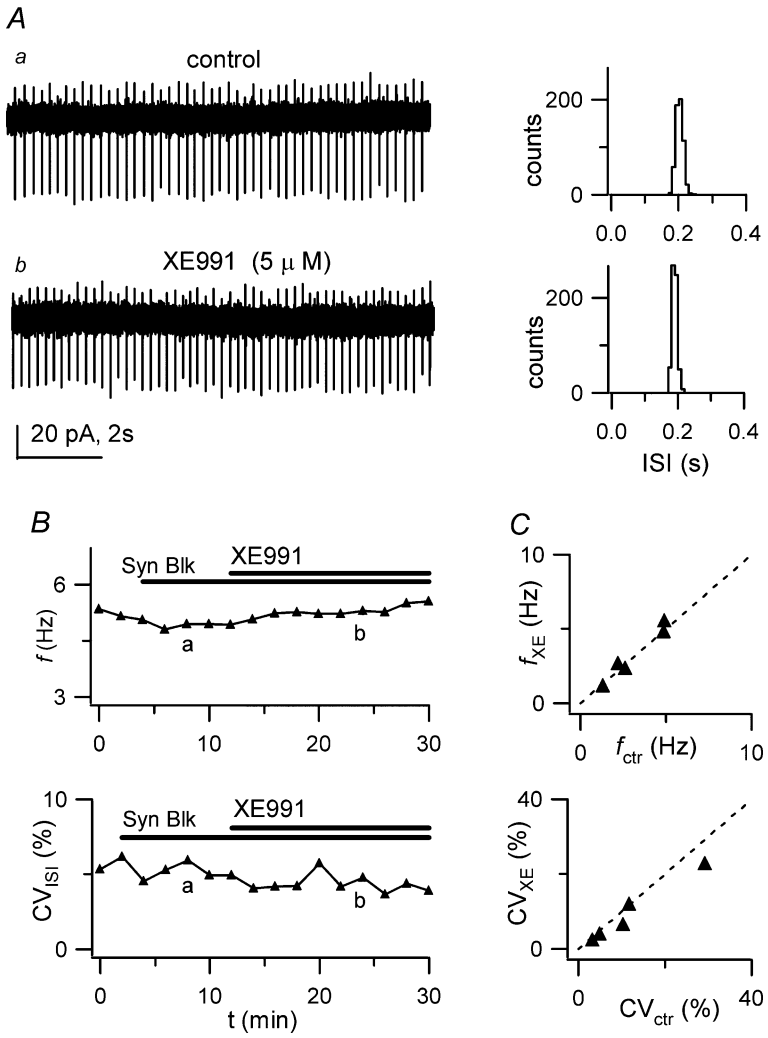


**Figure 8. XE991 has no effect on autorhythmicity**
*A*, left: LCA traces before (*a*) and after (*b*) bath application of 5 $\mu$M XE991, in the presence of synaptic blockers. Right, 1 min ISI distributions for traces on the left. Mean ISI and $CV_{ISI}$: 202 ms and 5.9% (upper histogram) and 180 ms and 3.9% (lower histogram). *B*, time course of $f$ (upper plot) and $CV_{ISI}$ (lower plot) for the recording shown in *A*, indicating no major $f$ or $CV_{ISI}$ changes during drug application. Horizontal bars indicate times of application of synaptic blockers and XE991; labels indicate time position of traces *a* and *b* shown in *A*. *C*, plot of $f$ (top) and $CV_{ISI}$ (bottom) in the presence of XE991 ($f_{XE}$, $CV_{XE}$), *vs* respective values in control ($f_{ctr}$, $CV_{ctr}$), for 5 cells.

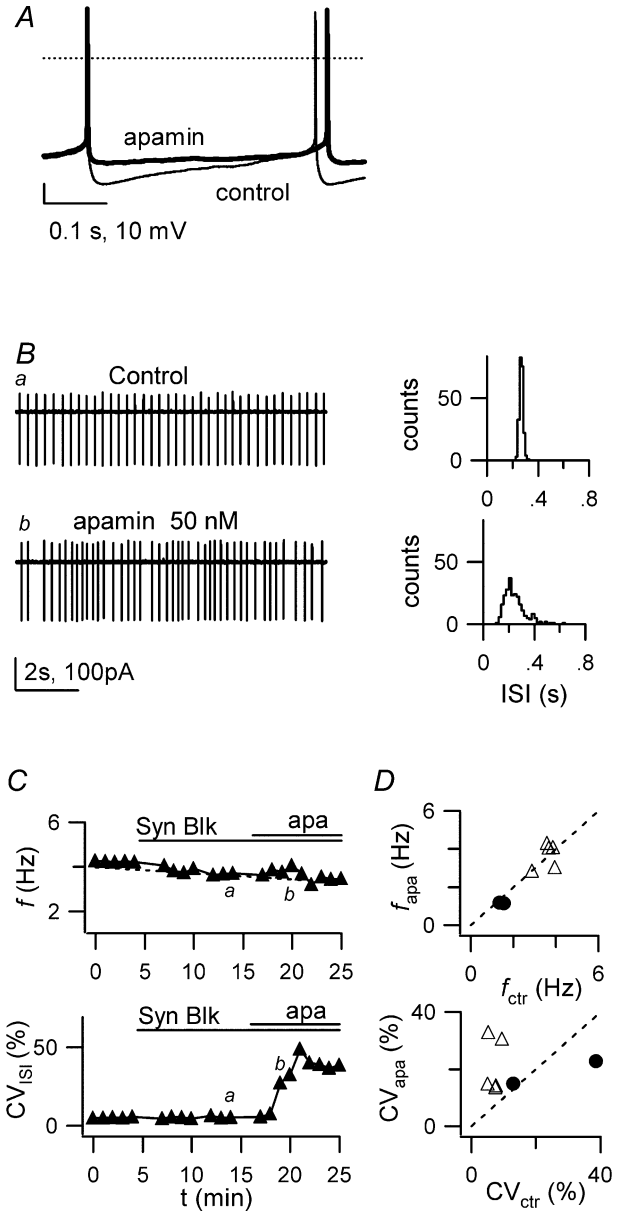


**Figure 9. Control of pacemaker precision by apamin**
Effects of the SK-type $Ca^{2+}$-dependent $K^+$ channel blocker apamin (50 nM). *A*, voltage traces from a WC current-clamp recording showing autorhythmic firing before (thin line) and 3 min after apamin application (thick line). Note the decrease of the spike AHP after apamin. Dotted line: 0 mV. Holding current −15 pA for both traces. *B*, LCA traces before (*a*) and during application of 50 nM apamin (*b*). Right, 1 min ISI distributions for traces on the left. Mean ISI and $CV_{ISI}$: 269 ms and 5.3% (upper histogram), 246 ms and 32.7% (lower histogram). Note $CV_{ISI}$ increase induced by apamin. *C*, time course of *f* (upper plot) and $CV_{ISI}$ (lower plot) for the recording in *B*. Bars indicate times of application of synaptic blockers and apamin; labels indicate time position of traces *a* and *b* shown in *B*. *D*, plot of *f* (top) and $CV_{ISI}$ (bottom) in the presence of apamin ($f_{apa}$, $CV_{apa}$) *vs* respective values in control ($f_{ctr}$, $CV_{ctr}$), for 7 cells. ● indicates 2 cells with $f < 2$ Hz where neither *f* nor $CV_{ISI}$ were affected by apamin.

might still be modulatory agents influencing pacemaking (e.g. acetylcholine, noradrenaline, or serotonin), an indication that slice conditions were compatible with those occurring *in vivo* comes from the observation that Golgi cells *in vivo* and *in vitro* fire rhythmically at similar frequencies.

GoC spontaneous firing frequency at physiological temperature (∼9 Hz on average) was slightly lower or similar to values measured in the rat *in vivo* (∼15 Hz, Schulman & Bloom, 1981; ∼8.4 Hz, Vos *et al.* 1999). Firing was much more regular in slices ($CV_{ISI}$ ∼0.1) than *in vivo* ($CV_{ISI}$ ∼0.9, Vos *et al.* 1999). The frequency and regularity of GoC activity *in vivo* is likely to be influenced by massive synaptic inputs, which are absent in slices because granule cells do not discharge spontaneously (D'Angelo *et al.* 1995) and afferent mossy fibres are deprived of their cell body. Accordingly, firing activity in slices was marginally altered by block of such inputs. Firing frequency and regularity were correlated, and were modulated in parallel by down-regulation of intrinsic currents relevant to pacemaking (with the exception of $I_{apa}$; see below). Firing regularity *in vivo* should thus be under dual control of synaptic inputs and the level of activity of pacemaker channels.

Because of their rhythmic firing at 1–10 Hz and the extended plexiform axonal arborization developing in the granular layer, the majority (81–87%) of large neurons in lobules II–VIII were identified as Golgi cells. It should be recalled that Lugaro cells, which might in some cases display a GoC-like soma located deep in the GL (Lainé & Axelrad, 2002), do not discharge spontaneously in slice preparations (Dieudonné & Dumoulin, 2000). The main electrophysiological properties of GoCs were homogeneous. However, we cannot rule out that a minority of large granular layer interneurons, excluded from this study because silent, irregularly firing or bursting, represent functionally different GoC subtypes; indeed, a few non-pacemaker neurons endowed with a Golgi-like plexiform axon were observed. The existence of GoC subtypes has been previously suggested on the basis of neurochemical studies (Geurts *et al.* 2001). The observation that, in a small fraction of cells characterized by low discharge frequency, apamin was ineffective on pacemaking, might also indicate the existence of distinct functional GoC subclasses.

In addition to autorhythmicity, which is the focus of the present study, GoCs revealed interesting dynamic behaviours, including the ability to (i) respond to a depolarizing input with high-frequency repetitive firing up to 200 Hz showing adaptation at increasing frequencies; and (ii) to produce a deep AHP following discharge. These properties match behaviours of GoCs *in vivo*, which can show sustained discharge at high frequency (up to 50 Hz, Edgley & Lidierth, 1987; 20–150 Hz, Miles *et al.* 1980). Following punctuate sensory stimulation, GoCs respond with short bursts of 2–3 spikes at up to 200–300 Hz

followed by a silent pause (Vos *et al.* 1999), which can therefore be due, at least in part, to intrinsic GoC electroresponsive properties. The presence of spike-frequency adaptation, together with rebound excitation following a hyperpolarization, suggests that GoCs are able to signal the time of input changes both in the excitatory and inhibitory direction; rebound excitation following hyperpolarization may contribute to resetting the phase of spontaneous firing (Chan *et al.* 2004).

## Membrane currents underlying Golgi cell autorhythmic firing

While looking for depolarizing current components contributing to the pacemaker depolarization in GoCs, we found evidence for the participation of $Na^+$ currents and $I_h$.

**Subthreshold $Na^+$ current.** A non-inactivating subthreshold $Na^+$ current is active in GoCs in the pacemaker range (positive to −70 mV), as shown here by the effect of TTX on the steady-state current measured with small voltage-clamp steps. A persistent $Na^+$ current of similar amplitude has been recorded recently in rat GoCs (J. Magistretti, unpublished results). This current is likely to play a critical role in driving autorhythmic firing, thus adding to the emerging evidence that $Na^+$ currents are major sources for the depolarizing drive to threshold in low-frequency rhythmic neurons (Pennartz *et al.* 1997; Feigenspan *et al.* 1998; Bevan & Wilson, 1999; Bennett *et al.* 2000; Beurrier *et al.* 2000; Taddese & Bean, 2002; Do & Bean, 2003; Jackson *et al.* 2004; see also Wilson & Callaway, 2000).

**Hyperpolarization-activated cationic current $I_h$.** The decrease of firing frequency induced in GoCs by ZD 7288 suggests that $I_h$ contributes to the subthreshold pacemaker depolarization, as found in other low-frequency pacemaker neurons (Maccaferri & McBain, 1996; Bennett *et al.* 2000; Neuhoff *et al.* 2002; Funahashi *et al.* 2003; Chan *et al.* 2004). The hypothesis that the effect of ZD 7288 on firing is mediated by block of hyperpolarizing $K^+$ conductances (Do & Bean, 2003) is ruled out in GoCs by the slow, gradual firing deceleration and the lack of firing arrest. $I_h$ was reported not to be involved in firing in some pacemaker neuronal types (Pennartz *et al.* 1997; Feigenspan *et al.* 1998; Bevan & Wilson, 1999; Taddese & Bean, 2002; Do & Bean, 2003; but see Beurrier *et al.* 2000), suggesting that in those neurons a relatively negative activation threshold prevents current build-up in the interspike voltage range. However, $I_h$ activation threshold and half-activation potential are variable across cell types (Pape, 1996). Given the role of $I_h$ in GoC pacemaking, its activation threshold in these neurons should be relatively positive.

**M-type $K^+$ current.** We showed that GoC excitability is decreased by application of low doses (5 $\mu$M) of the anticonvulsant drug retigabine. At this dose, retigabine is an agonist at recombinant homomeric and heteromeric channels formed with KCNQ2–5 (Main *et al.* 2000; Wickenden *et al.* 2000; Tatulian *et al.* 2001; Dupuis *et al.* 2002) and increases native $I_M$ in sympathetic neurons (Wickenden *et al.* 2000; Tatulian *et al.* 2001; Passmore *et al.* 2003). Low retigabine doses are ineffective on $Na^+$ and $Ca^{2+}$ currents (Rundfeldt & Netzer, 2000). A potentiation of $GABA_A$ receptor activity has been reported (Rundfeldt & Netzer, 2000); however, the latter should not significantly influence the effect in GoCs reported here, which was obtained in the presence of saturating doses of the $GABA_A$ antagonist gabazine. Thus the observed retigabine effect argues in favour of the functional presence of a retigabine-sensitive, KCNQ-mediated M-type current in GoCs.

We also show that low doses (5 $\mu$M) of the $I_M$ antagonist XE991 have no effect on pacemaking. This was unexpected given the suggested presence of $I_M$ in GoCs. It was reported that XE991 block is voltage dependent in sympathetic neurons (Romero *et al.* 2004), being more effective at positive (−30 mV) potentials. However, effects of XE991 on cells maintained in resting, hyperpolarized conditions have also been reported (Yu & Yaari, 2004; Gu *et al.* 2005). It is therefore questionable whether the lack of effect of XE991 on spontaneous firing in GoCs is due to voltage dependence of $I_M$ block. The phenomenon could alternatively be explained if the suggested retigabine-sensitive current was XE991 insensitive and/or was not involved in control of autorhythmic firing properties. The latter hypothesis seems unlikely given that the current is involved in control of threshold excitability (Fig. 7). As a consequence, we hypothesize that the retigabine-sensitive current in GoCs is not sensitive to low XE991 doses. This raises the problem of the molecular identity of such current. The precise molecular profile of KCNQ-containing retigabine targets in GoCs is unknown, and their XE991 sensitivity might be influenced by coassembled accessory subunits. KCNQ5 mRNA is present in the rat GL (Schroeder *et al.* 2000), and KCNQ5 homomeric recombinant channels are reported to have low sensitivity to XE991 block (Schroeder *et al.* 2000). Further studies including direct recording of retigabine-sensitive current will be necessary to clarify these subjects.

**SK-type $Ca^{2+}$-dependent $K^+$ currents.** Apamin disrupted firing regularity, showing that apamin-sensitive $Ca^{2+}$-dependent $K^+$ channels from the SK family are essential for generating highly precise pacemaking in GoCs. This is similar to observations in other low-frequency pacemaker neurons (Shepard & Bunney, 1988; reviewed in Stocker, 2004). Saturating apamin doses

for SK channels did not significantly alter the average firing frequency, in line with other reports (Bennett *et al.* 2000; Hallworth *et al.* 2003; but see Wolfart *et al.* 2001). Apamin-induced irregular firing could arise from spike clustering induced by suppression of the single-spike AHP.

### A synthesis of mechanisms

Our observations allow us to propose a hypothesis on the mechanism of GoC pacemaking. For convenience, we begin our description from the ISI. During the AHP (trough below −70 mV), $I_h$ slowly activates, raising membrane potential enough (above −70 mV) to activate $I_{Na,sub}$. The joint action of $I_h$ and $I_{Na,sub}$ leads membrane voltage to threshold for a new spike. Depolarization activates repolarizing feedback mechanisms with different kinetics, both fast (the spike repolarization mechanism) and slow ($I_h$ deactivation). The slowly activating and deactivating $I_h$, coupled to faster currents, is in principle sufficient to generate slow $V_m$ oscillations (e.g. Dickson *et al.* 2000; Hutcheon & Yarom, 2000). However, it is clear that activation of additional currents with slow voltage-dependent kinetics would sustain slow GoC pacing and increase the repertoire of modulatory actions enabling tuning of pacemaker properties. Therefore, a special interest is raised by the M-like $K^+$ current for which we have proposed the functional expression in GoCs and which may concur to generate and reinforce the repolarizing phase. The SK-mediated $I_{apa}$ proved unable to regulate the average frequency, but seems to play an important role in stabilizing the cycle.

Although the proposed mechanism is in line with experimental observations in other pacemaker neurons (e.g. Bennett *et al.* 2000) and explains the ability to sustain autorhythmic firing, several questions remain open. The role of $I_{Na,sub}$ and M-like currents in GoC pacemaking awaits an experimental demonstration. The $K^+$ current $I_A$ (see Midtgaard, 1992; Liss *et al.* 2001) could also contribute to contrasting the depolarizing action of $I_{Na,sub}$ and $I_h$ and to control firing frequency. Finally, low-threshold voltage-dependent $Ca^{2+}$ currents could contribute to subthreshold depolarization (Wilson & Callaway, 2000; Jackson *et al.* 2004; Pignatelli *et al.* 2005). The role of these channels should be investigated. The assessment of the interplay between the various voltage-dependent conductances would also benefit from a realistic numerical simulation of the present hypothesis.

### Conclusions and functional implications

Low-frequency pacemaking in GoCs suggests specific consequences for cerebellar operating mechanisms. Intrinsic firing can be up- or downregulated, depending on the nature of synaptic inputs. GoCs may therefore behave as sensitive detectors both for excitation carried by mossy and parallel fibres and for inhibition relayed by various interneurons (including Lugaro and stellate cells). The rhythmic activity of GoCs could contribute to determining both cyclic and tonic inhibition of granule cells. Tonic inhibition has a TTX-sensitive component (Rossi *et al.* 2003), whose intensity is likely to be regulated by the frequency of GoC activity through slow integration of GABA spillover in the glomerulus. Cyclic inhibition could contribute to explaining the population oscillations observed in the cerebellar granular layer of awake resting animals (Pellerin & Lamarre, 1997; Hartmann & Bower, 1998). These oscillations could also involve other network properties. Indeed, the parallel fibre feedback through GoCs has itself the ability to convert a steady mossy fibre input into a cyclic Golgi and granule cell discharge (Maex & De Schutter, 1998). Moreover, since granule cells are resonant at $\theta$-frequency (D'Angelo *et al.* 2001), the effects of GoCs' cyclic inhibition would be that of tuning granule cells to a preferential input frequency band. Modulation of the multiple currents sustaining autorhythmicity could regulate the GoC functional state and consequently affect the frequency and regularity of population oscillations.

## References

Bennett BD, Callaway JC & Wilson CJ (2000). Intrinsic membrane properties underlying spontaneous tonic firing in neostriatal cholinergic interneurons. *J Neurosci* **20**, 8493–8503.

Beurrier C, Bioulac B & Hammond C (2000). Slowly inactivating sodium current (I(NaP) underlies single-spike activity in rat subthalamic neurons. *J Neurophysiol* **83**, 1951–1957.

Bevan MD & Wilson CJ (1999). Mechanisms underlying spontaneous oscillation and rhythmic firing in rat subthalamic neurons. *J Neurosci* **19**, 7617–7628.

Brown DA & Adams PR (1980). Muscarinic suppression of a novel voltage-sensitive $K^+$ current in a vertebrate neuron. *Nature* **283**, 673–676.

Brown BS & Yu SP (2000). Modulation and genetic identification of the M-channel. *Prog Biophys Mol Biol* **73**, 135–166.

Bureau I, Dieudonné S, Coussen F & Mulle C (2000). Kainate receptor-mediated synaptic currents in cerebellar Golgi cells are not shaped by diffusion of glutamate. *Proc Natl Acad Sci U S A* **97**, 6838–6843.

Chan CS, Shigemoto R, Mercer JN & Surmeier DJ (2004). HCN2 and HCN1 channels govern the regularity of autonomous pacemaking and synaptic resetting in globus pallidus neurons. *J Neurosci* **24**, 9921–9932.

Cooper EC, Harrington E, Jan YN & Jan LY (2001). M Channel KCNQ2 subunits are localized to key sites for control of neuronal network oscillations and synchronization in mouse brain. *J Neurosci* **21**, 9529–9540.

D'Angelo E, De Filippi G, Rossi P & Taglietti V (1995). Synaptic excitation of individual rat cerebellar granule cells in situ: evidence for the role of NMDA receptors. *J Physiol* **484**, 397–413.

D'Angelo E, Nieus T, Maffei A, Armano S, Rossi P, Taglietti V, Fontana A & Naldi G (2001). Theta-frequency bursting and resonance in cerebellar granule cells: experimental evidence and modeling of a slow $K^+$-dependent mechanism. *J Neurosci* **21**, 759–770.

Dickson CT, Magistretti J, Shalinsky MH, Fransen E, Hasselmo ME & Alonso A (2000). Properties and role of I(h) in the pacing of subthreshold oscillations in entorhinal cortex layer II neurons. *J Neurophysiol* **83**, 2562–2579.

Dieudonné S (1995). Glycinergic synaptic currents in Golgi cells of the rat cerebellum. *Proc Natl Acad Sci U S A* **92**, 1441–1445.

Dieudonné S (1998). Submillisecond kinetics and low efficacy of parallel fibre-Golgi cell synaptic currents in the rat cerebellum. *J Physiol* **510**, 845–866.

Dieudonné S & Dumoulin A (2000). Serotonin-driven long-range inhibitory connections in the cerebellar cortex. *J Neurosci* **20**, 1837–1848.

Do MT & Bean BP (2003). Subthreshold sodium currents and pacemaking of subthalamic neurons: modulation by slow inactivation. *Neuron* **39**, 109–120.

Dugué GP, Dumoulin A, Triller A & Dieudonné S (2005). Target-dependent use of coreleased inhibitory transmitters at central synapses. *J Neurosci* **25**, 6490–6498.

Dupuis DS, Schroder RL, Jespersen T, Christensen JK, Christophersen P, Jensen BS & Olesen SP (2002). Activation of KCNQ5 channels stably expressed in HEK293 cells by BMS-204352. *Eur J Pharmacol* **437**, 129–137.

Eccles JC, Ito M & Szentágothai J (1967). *The Cerebellum as a Neuronal Machine*. Springer, Berlin.

Edgley SA & Lidierth M (1987). The discharges of cerebellar Golgi cells during locomotion in the cat. *J Physiol* **392**, 315–332.

Feigenspan A, Gustincich S, Bean BP & Raviola E (1998). Spontaneus activity of solitary dopaminergic cell of the retina. *J Neurosci* **18**, 6776–6789.

Funahashi M, Mitoh Y, Kohjitani A & Matsu R (2003). Role of the hyperpolarization-activated cation current ($I_h$) in pacemaker activity in area postrema neurons of rat brain slices. *J Physiol* **552**, 135–148.

Garcia ML, Hanner M, Knaus HG, Koch R, Schmalhofer W, Slaughter RS & Kaczorowski GJ (1997). Pharmacology of potassium channels. *Adv Pharmacol* **39**, 425–471.

Gasparini S & DiFrancesco D (1997). Action of the hyperpolarization-activated current ($I_h$) blocker ZD 7288 in hippocampal CA1 neurons. *Pflugers Arch* **435**, 99–106.

Geurts FJ, Timmermans J, Shigemoto R & De Schutter E (2001). Morphological and neurochemical differentiation of large granular layer interneurons in the adult rat cerebellum. *Neuroscience* **104**, 499–512.

Golgi C (1883). Sulla fina anatomia degli organi centrali del sistema nervoso IV. Sulla fina anatomia delle circonvoluzioni cerebellari. *Riv Sper Freniatr Med Leg Alien Ment* **9**, 1–17.

Gu N, Vervaeke K, Hu H & Storm JF (2005). Kv7/KCNQ/M and HCN/h, but not KCa2/SK channels, contribute to the somatic medium after-hyperpolarization and excitability control in CA1 hippocampal pyramidal cells. *J Physiol* **566**, 689–715.

Hallworth NE, Wilson CJ & Bevan MD (2003). Apamin-sensitive small conductance calcium-activated potassium channels, through their selective coupling to voltage-gated calcium channels, are critical determinants of the precision, pace, and pattern of action potential generation in rat subthalamic nucleus neurons *in vitro*. *J Neurosci* **23**, 7525–7542.

Hartmann MJ & Bower JM (1998). Oscillatory activity in the cerebellar hemispheres of unrestrained rats. *J Neurophysiol* **80**, 1598–1604.

Hutcheon B & Yarom Y (2000). Resonance, oscillation and the intrinsic frequency preferences of neurons. *Trends Neurosci* **23**, 216–222.

Ishii TM, Maylie J & Adelman JP (1997). Determinants of apamin and d-tubocurarine block in SK potassium channels. *J Biol Chem* **272**, 23195–23200.

Jackson AC, Yao GL & Bean BP (2004). Mechanism of spontaneous firing in dorsomedial suprachiasmatic nucleus neurons. *J Neurosci* **24**, 7985–7998.

Jentsch TJ (2000). Neuronal KCNQ potassium channels: physiology and role in disease. *Nat Rev Neurosci* **1**, 21–30.

Knoflach F, Woltering T, Adam G, Mutel V & Kemp JA (2001). Pharmacological properties of native metabotropic glutamate receptors in freshly dissociated Golgi cells of the rat cerebellum. *Neuropharmacology* **40**, 163–169.

Kohler M, Hirschberg B, Bond CT, Kinzie JM, Marrion NV, Maylie J & Adelman JP (1996). Small-conductance, calcium-activated potassium channels from mammalian brain. *Science* **273**, 1709–1714.

Lainé J & Axelrad H (2002). Extending the cerebellar Lugaro cell class. *Neuroscience* **115**, 363–374.

Liss B, Franz O, Sewing S, Bruns R, Neuhoff H & Roeper J (2001). Tuning pacemaker frequency of individual dopaminergic neurons by Kv4.3L and KChip3.1 transcription. *EMBO J* **20**, 5715–5724.

Llinás R (1988). The intrinsic electrophysiological properties of mammalian neurons: insights into central nervous system function. *Science* **242**, 1654–1664.

Lugaro E (1894). Sulle connessioni tra gli elementi nervosi della corteccia cerebellare con considerazioni generali sul significato fisiologico dei rapporti tra gli elementi nervosi. *Riv Sper Freniatr Med Leg Alien Ment* **20**, 297–331.

Maccaferri G & McBain CJ (1996). The hyperpolarization-activated current ($I_h$) and its contribution to pacemaker activity in rat CA1 hippocampal stratum oriens-alveus interneurones. *J Physiol* **497**, 119–130.

Maex R & De Schutter E (1998). Synchronization of golgi and granule cell firing in a detailed network model of the cerebellum granule cell layer. *J Neurophysiol* **80**, 2521–2537.

Main MJ, Cryan JE, Dupere JR, Cox B, Clare JJ & Burbidge SA (2000). Modulation of KCNQ2/3 potassium channels by the novel anticonvulsant retigabine. *Mol Pharmacol* **58**, 253–262.

Midtgaard J (1992). Membrane properties and synaptic responses of Golgi cells and stellate cells in the turtle cerebellum *in vitro*. *J Physiol* **457**, 329–354.

Miles FA, Fuller JH, Braitman DJ & Dow BM (1980). Long-term adaptive changes in primate vestibuloocular reflex. III. Electrophysiological observations in flocculus of normal monkeys. *J Neurophysiol* **43**, 1437–1476.

Misra C, Brickley SG, Farrant M & Cull-Candy SG (2000). Identification of subunits contributing to synaptic and extrasynaptic NMDA receptors in Golgi cells of the rat cerebellum. *J Physiol* **524**, 147–162.

Mugnaini E & Floris A (1994). The unipolar brush cell: a neglected neuron of the mammalian cerebellar cortex. *J Comp Neurol* **339**, 174–180.

Neher E (1992). Correction for liquid junction potentials in patch clamp experiments. *Meth Enzymol* **207**, 123–131.

Neuhoff H, Neu A, Liss B & Roeper J (2002). I(h) channels contribute to the different functional properties of identified dopaminergic subpopulations in the midbrain. *J Neurosci* **22**, 1290–1302.

Notomi T & Shigemoto R (2004). Immunohistochemical localization of $I_h$ channel subunits, HCN1–4, in the rat brain. *J Comp Neurol* **471**, 241–276.

Oliver D, Knipper M, Derst C & Fakler B (2003). Resting potential and submembrane calcium concentration of inner hair cells in the isolated mouse cochlea are set by KCNQ-type potassium channels. *J Neurosci* **23**, 2141–2149.

Pape H (1996). Queer current and pacemaker: the hyperpolarization-activated cation current in neurons. *Annu Rev Physiol* **58**, 299–327.

Passmore GM, Selyanko AA, Mistry M, Al-Qatari M, Marsh SJ, Matthews EA, Dickenson AH, Brown TA, Burbidge SA, Main M & Brown DA (2003). KCNQ/M currents in sensory neurons: significance for pain therapy. *J Neurosci* **23**, 7227–7236.

Pellerin JP & Lamarre Y (1997). Local field potential oscillations in primate cerebllar cortex during voluntary movement. *J Neurophysiol* **78**, 3502–3507.

Pennartz CM, Bierlaagh MA & Geurtsen AM (1997). Cellular mechanisms underlying spontaneous firing in rat suprachiasmatic nucleus: involvement of a slowly inactivating component of sodium current. *J Neurophysiol* **78**, 1811–1825.

Pignatelli A, Kobayashi K, Okano H & Belluzzi O (2005). Functional properties of dopaminergic neurones in the mouse olfactory bulb. *J Physiol* **564**, 501–514.

Ramirez JM, Tryba AK & Pena F (2004). Pacemaker neurons and neuronal networks: an integrative view. *Curr Opin Neurobiol* **14**, 665–674.

Robbins J (2001). KCNQ potassium channels: physiology, pathophysiology, and pharmacology. *Pharmacol Ther* **90**, 1–19.

Romero M, Reboreda A, Sanchez E & Lamas JA (2004). Newly developed blockers of the M-current do not reduce spike frequency adaptation in cultured mouse sympathetic neurons. *Eur J Neurosci* **19**, 2693–2702.

Rossi DJ, Hamann M & Attwell D (2003). Multiple modes of GABAergic inhibition of rat cerebellar granule cells. *J Physiol* **548**, 97–110.

Rossi P, Mapelli L, Roggeri L, Gall D, de Kerchuve d'Exaerde A, Schiffman SN, Taglietti V & D'Angelo E (2006). Long lasting inhibition of constitutive inward rectifyer currents in cerebellar granule cells by synaptic activation of GABAB receptors. *Eur J Neurosci* in press.

Rundfeldt C & Netzer R (2000). The novel anticonvulsant retigabine activates M-currents in Chinese hamster ovary-cells tranfected with human KCNQ2/3 subunits. *Neurosci Lett* **282**, 73–76.

Saganich MJ, Machado E & Rudy B (2001). Differential expression of genes encoding subthreshold-operating voltage-gated $K^+$ channels in brain. *J Neurosci* **21**, 4609–4626.

Santoro B, Chen S, Luthi A, Pavlidis P, Shumyatski GP, Tibbs GR & Siegelbaum SA (2000). Molecular and functional heterogeneity of hyperpolarization-activated pacemaker channels in the mouse CNS. *J Neurosci* **20**, 5264–5275.

Schroeder BC, Hechenberger M, Weinreich F, Kubisch C & Jentsch TJ (2000). KCNQ5, a novel potassium channel broadly expressed in brain, mediates M-type currents. *J Biol Chem* **275**, 24089–24095.

Schulman JA & Bloom FE (1981). Golgi cells of the cerebellum are inhibited by inferior olive activity. *Brain Res* **210**, 350–355.

Shepard PD & Bunney BS (1988). Effects of apamin on the discharge properties of putative dopamine-containing neurons in vitro. *Brain Res* **463**, 380–384.

Singer W (1993). Synchronization of cortical activity and its putative role in information processing and learning. *Annu Rev Physiol* **55**, 349–374.

Stocker M (2004). $Ca^{2+}$-activated $K^+$ channels: molecular determinants and function of the SK family. *Nat Rev Neurosci* **5**, 758–770.

Stocker M & Pedarzani P (2000). Differential distribution of three Ca(2+)-activated K(+) channel subunits, SK1, SK2, and SK3, in the adult rat central nervous system. *Mol Cell Neurosci* **15**, 476–493.

Surmeier DJ, Mercer JN & Chan CS (2005). Autonomous pacemakers in the basal ganglia: who needs excitatory synapses anyway? *Curr Opin Neurobiol* **15**, 312–318.

Taddese A & Bean BP (2002). Subthreshold sodium current from rapidly inactivating sodium channels drives spontaneous firing of tuberomamillary neurons. *Neuron* **33**, 587–600.

Tatulian L, Delmas P, Abogadie FC & Brown DA (2001). Activation of expressed KCNQ potassium currents and native neuronal M-type potassium currents by the anti-convulsant drug retigabine. *J Neurosci* **21**, 5535–5545.

Turgeon SM & Albin RL (1993). Pharmacology, distribution, cellular localization and development of $GABA_B$ binding in rodent cerebellum. *Neuroscience* **55**, 311–323.

Vos BP, Maex R, Volny-Luraghi A & De Schutter E (1999). Cerebellar Golgi cells in the rat: receptive fields and timing of responses to facial stimulation. *Eur J Neurosci* **11**, 2621–2634.

Wang HS, Pan ZM, Shi WM, Brown BS, Wymore RS, Cohen IS, Dixon JE & McKinnon D (1998). KCNQ2 and KCNQ3 potassium channel subunits: molecular correlates of the M-channel. *Science* **282**, 1890–1893.

Wang XJ & Rinzel J (1999). Oscillatory and bursting properties of neurons. In *The Handbook of Brain Theory and Neuronal Networks*, ed. Arbib MA, pp. 686–691. MIT Press, London.

Watanabe D & Nakanishi S (2003). mGluR2 postsynaptically senses granule cell inputs at Golgi cell synapses. *Neuron* **39**, 821–829.

White JA, Sekar NS & Kay AR (1995). Errors in persistent inward currents generated by space-clamp errors: a modeling study. *J Neurophysiol* **73**, 2369–2377.

Wickenden AD, Yu W, Zou A, Jegla T & Wagoner PK (2000). Retigabine, a novel anti-convulsant, enhances activation of KCNQ2/Q3 potassium channels. *Mol Pharmacol* **58**, 591–600.

Wickenden AD, Zou A, Wagoner PK & Jegla T (2001). Characterization of KCNQ5/Q3 potassium channels expressed in mammalian cells. *Br J Pharmacol* **132**, 381–384.

Wilson CJ & Callaway JC (2000). Coupled oscillator model of the dopaminergic neuron of the substantia nigra. *J Neurophysiol* **83**, 3084–3100.

Wolfart J, Neuhoff H, Franz O & Roeper J (2001). Differential expression of the small conductance, calcium-activated potassium channel SK3 is critical for pacemaker control in dopaminergic midbrain neurons. *J Neurosci* **21**, 3443–3456.

Yue C & Yaari Y (2004). KCNQ/M channels control spike afterdepolarization and burst generation in hippocampal neurons. *J Neurosci* **24**, 4614–4624.

## Acknowledgements

We thank Dr J. Magistretti for comments on the manuscript and Dr M. Taglialatela for kindly providing retigabine and XE991. This work was supported by EU programs FP5-LIFE BIO4CT98-0182 'CEREBELLUM', FP5-IST35271 'SPIKEFORCE', FP6-IST028056 'SENSOPAC' and by Fondazione CARIPLO of Italy.